Electronic Supplementary Material (ESI) for Chemical Science.
This journal is © The Royal Society of Chemistry 2016

Supporting Information for

Symmetry of Octacoordination Environment has a Substantial Influence on Dinuclear Tb^{III} Triple-Decker Single-Molecule Magnets

Keiichi Katoh,[a,b]* Brian K. Breedlove[a,b] and Masahiro Yamashita[a,b]*

[a] Department of Chemistry, Graduate School of Science, Tohoku University, 6-3 Aramaki Aza Aoba, Aoba-ku, Sendai, Miyagi 980-8578, Japan.
[b] CREST, JST, 4-1-8 Honcho, Kawaguchi, Saitama 332-0012, Japan.

CONTACT AUTHOR
Phone; +81-22-795-3878. Fax: +81-22-795-3878.
E-mail: kkatoh@m.tohoku.ac.jp (KK)

Table of Contents

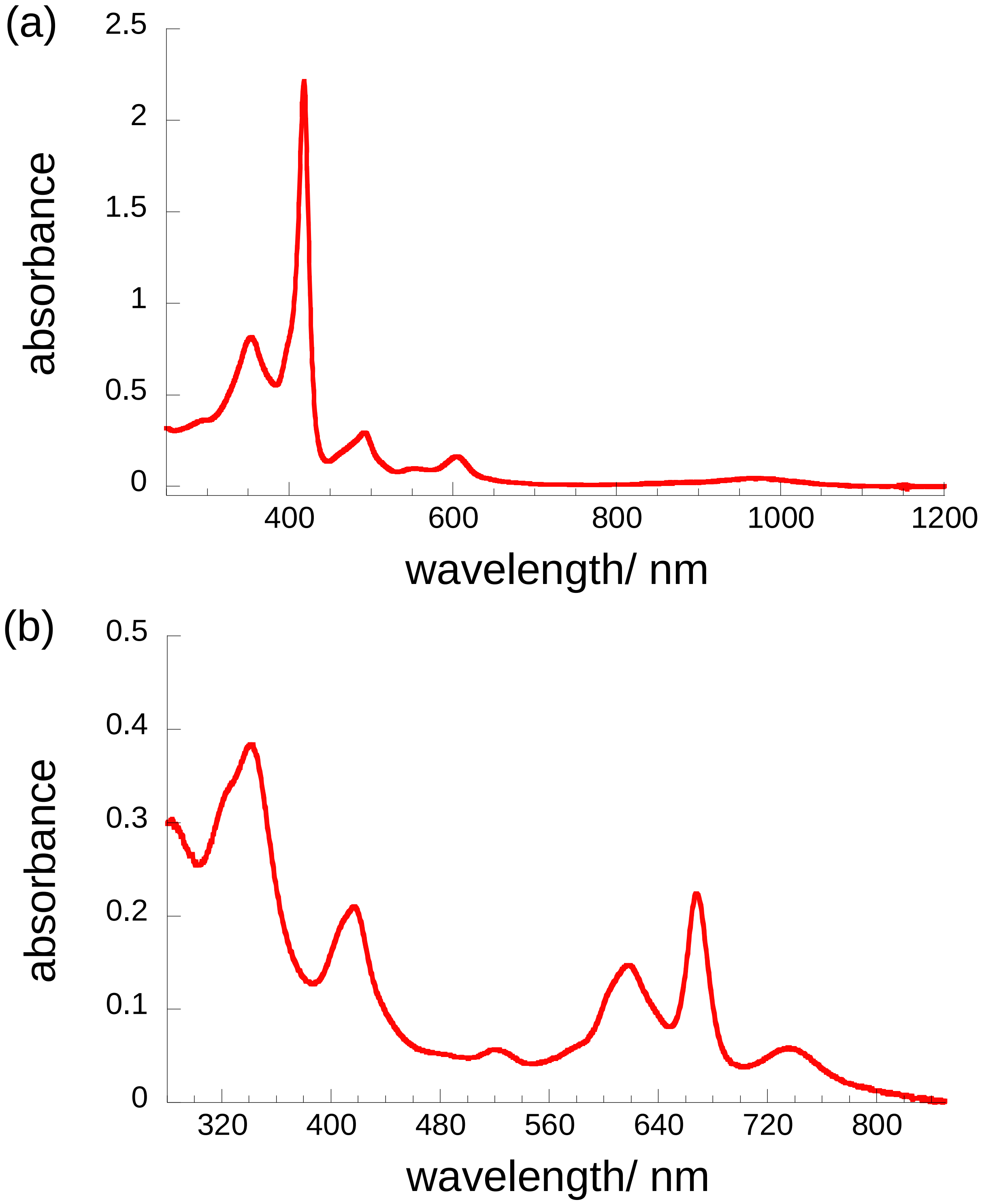

Fig. S1 Electronic spectra of (a) **1** and (b) **2** in $CHCl_3$ at 289 K.

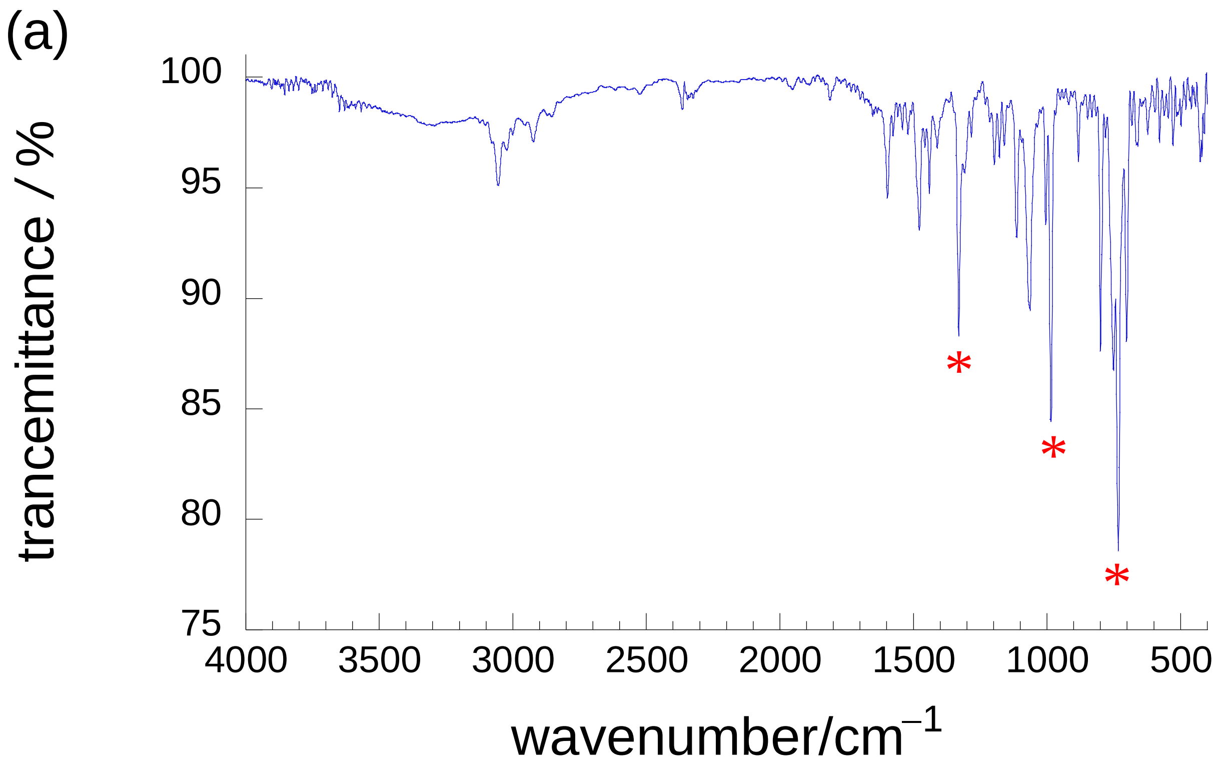

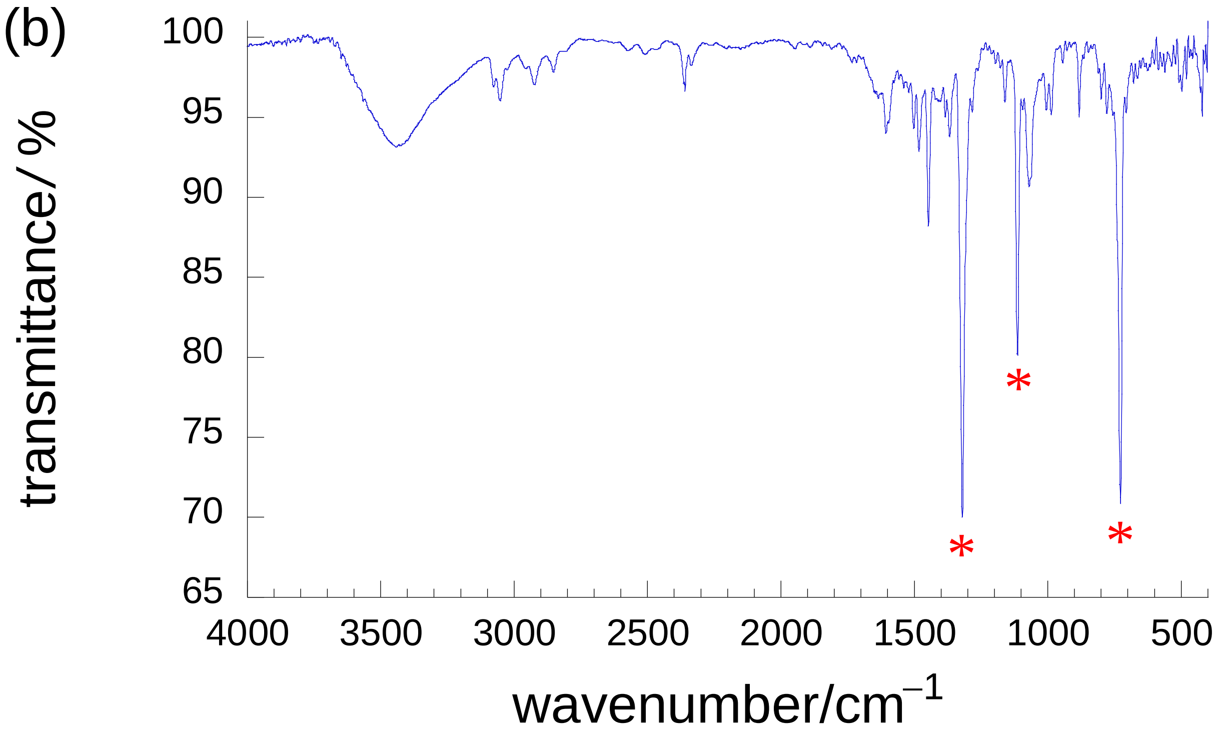

Fig. S2 FT-IR spectra of (a) **1** and (b) **2** as KBr pellets at 289 K. Three main strong peaks (*) at 1330, 1062, 728 cm^{-1} were assigned to the Pc^{2-}.[1]

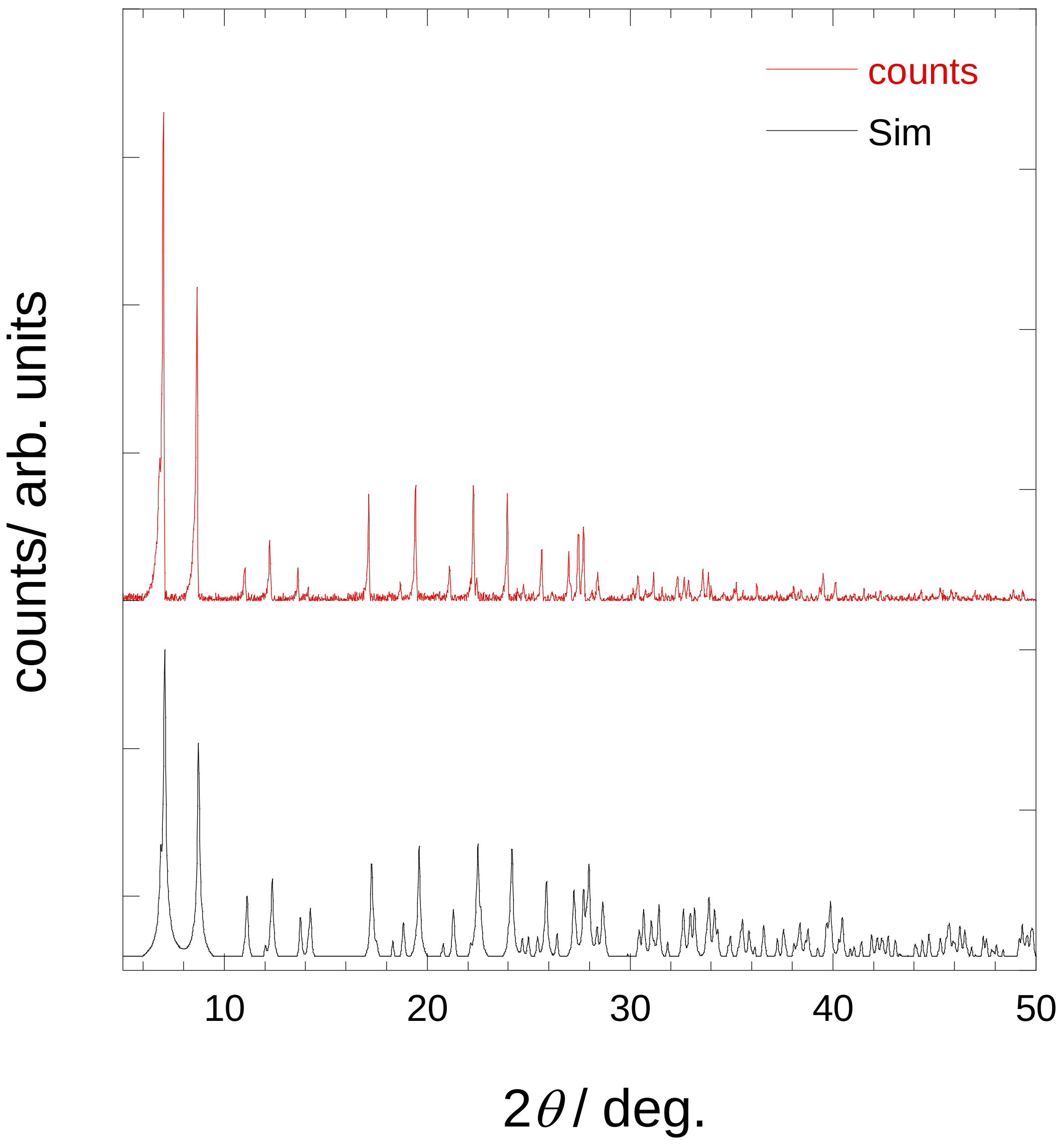

Fig. S3-1 PXRD patterns of **1** at 293 K.

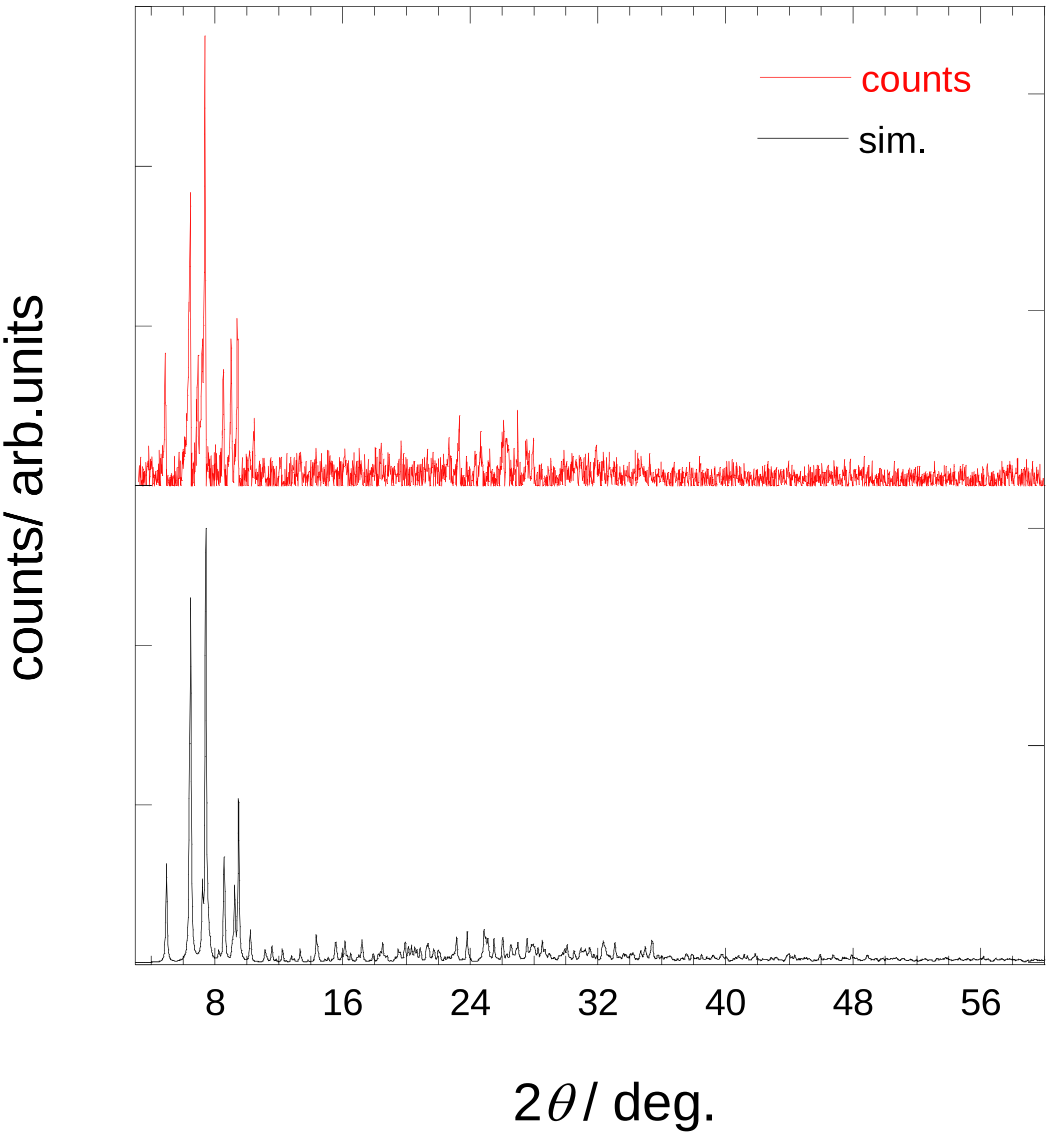

Fig. S3-2 PXRD patterns of **2** at 293 K.

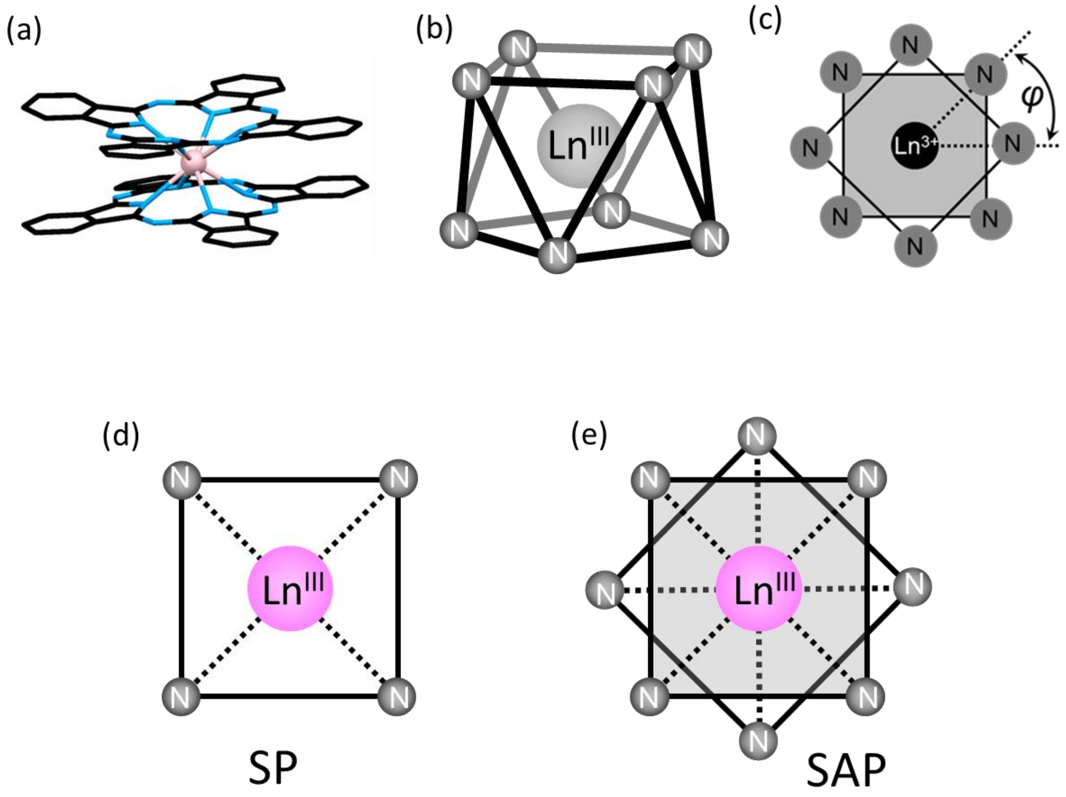

Fig. S4 (a) Molecular structure of $TbPc_2$. (b) Schematic illustration of the square-antiprismatic (SAP) coordination environment of $LnPc_2$. (c) Twist angle φ in SAPs in multiple-decker Ln^{III}-Pc complexes. (d) The square-prismatic (SP) coordination environment have D_{4h} point symmetry. (e) The square-antiprismatic (SAP) coordination environment have D_{4d} symmetry.

Table S1. Selected crystallographic data for **1**–**3**

	1 (CCDC 989974)	**2** (CCDC 1041202)	**3** (CCDC 753306)
Chemical formula	$C_{124}H_{72}N_{16}Cl_{12}Tb_2$	$C_{110}H_{62}N_{20}Cl_6Tb_2$	$C_{196}H_{250}N_{24}O_{26}Tb_2$
Formula weight	2529.22	2194.34	3678.06
T/K	93	93	93
Crystal system	tetragonal	monoclinic	triclinic
Space group	$I4/m$	$P2_1/c$	P–1
a/ nm	1.4314(6)	1.3800(3)	1.31648(11)
b/ nm	1.4314(6)	2.7638(6)	1.78266(17)
c/ nm	2.5736(12)	2.3522(5)	2.06226(19)
α/ deg.	90.00	90.00	107.2150(10)
β/ deg.	90.00	98.391(3)	90.5010(10)
γ/ deg.	90.00	90.00	100.8480(10)
V/ nm^3	5.273(4)	8.876(3)	4.5296(7)
Z	2	4	1
$R_1(I > 2s(I))$	0.0296	0.0761	0.0470
wR_2(all)	0.0888	0.1859	0.1357
GOF	1.219	1.109	1.088

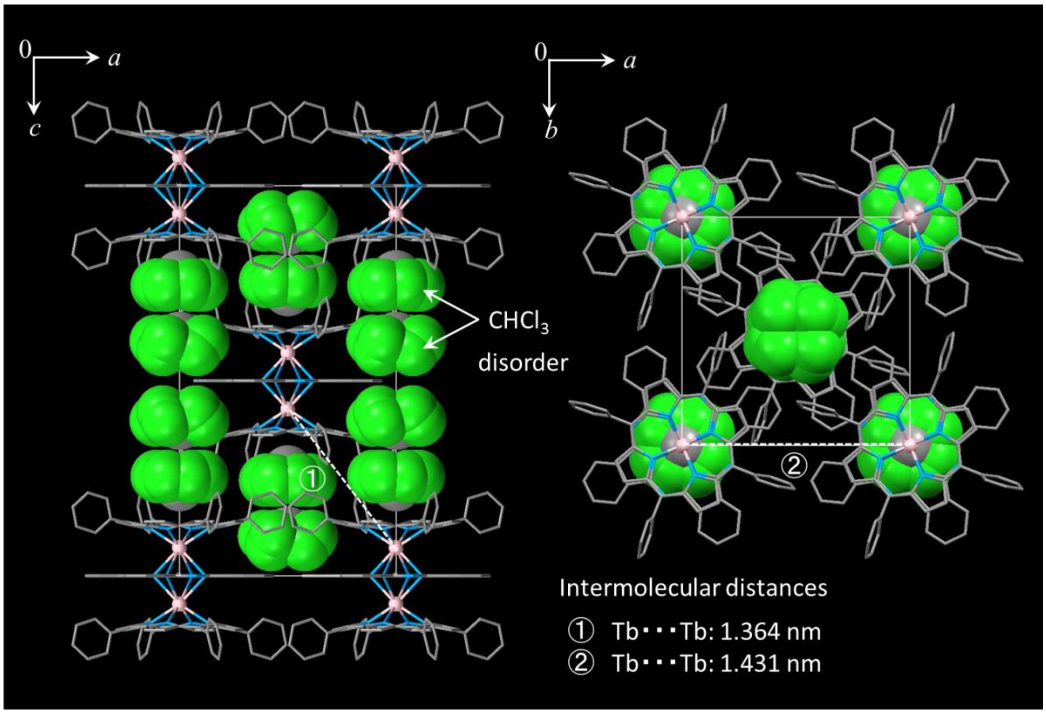

Fig. S5 Packing diagram of **1**. C_4 symmetrical disorder of the chloride atoms on chloroform is observed. The chloroform has C_{3v} symmetry. The unusual C_4 symmetry of chloroform observed in the single crystal of **1** is related to the strong intermolecular CH/n interactions between the chloroform and the point group D_4 (it has one C_4 axis) symmetric TTP ligand in **1**.

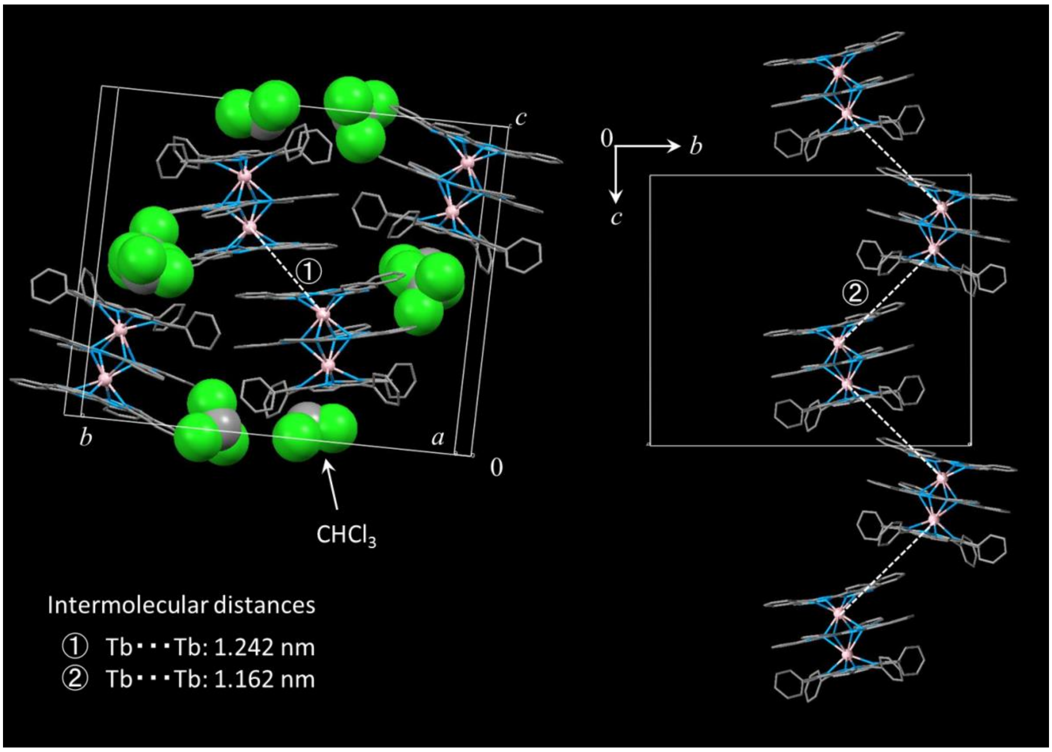

Fig. S6-1 Packing diagram for **2**.

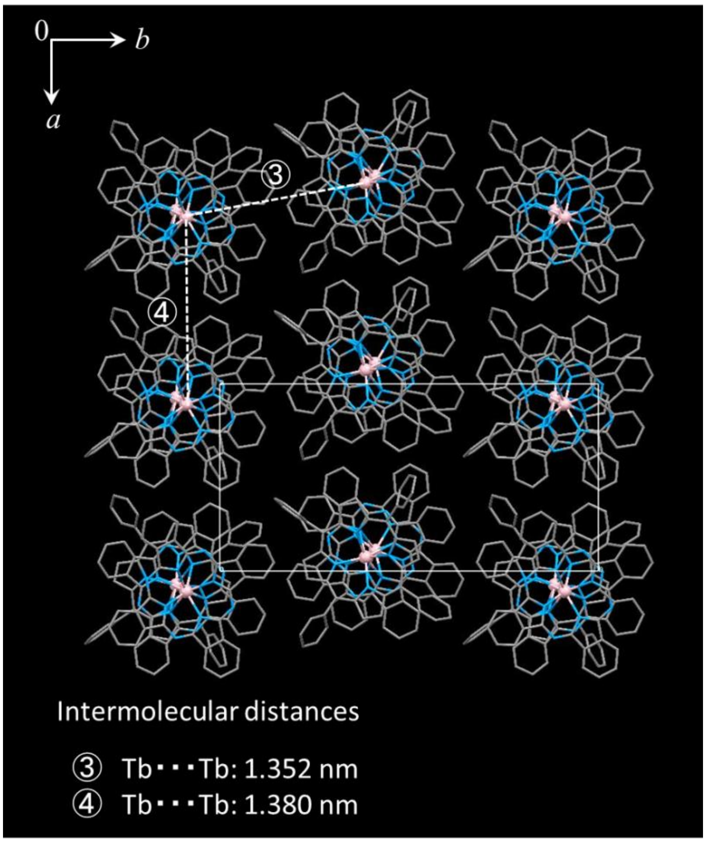

Fig. S6-2 Packing diagram for **2**.

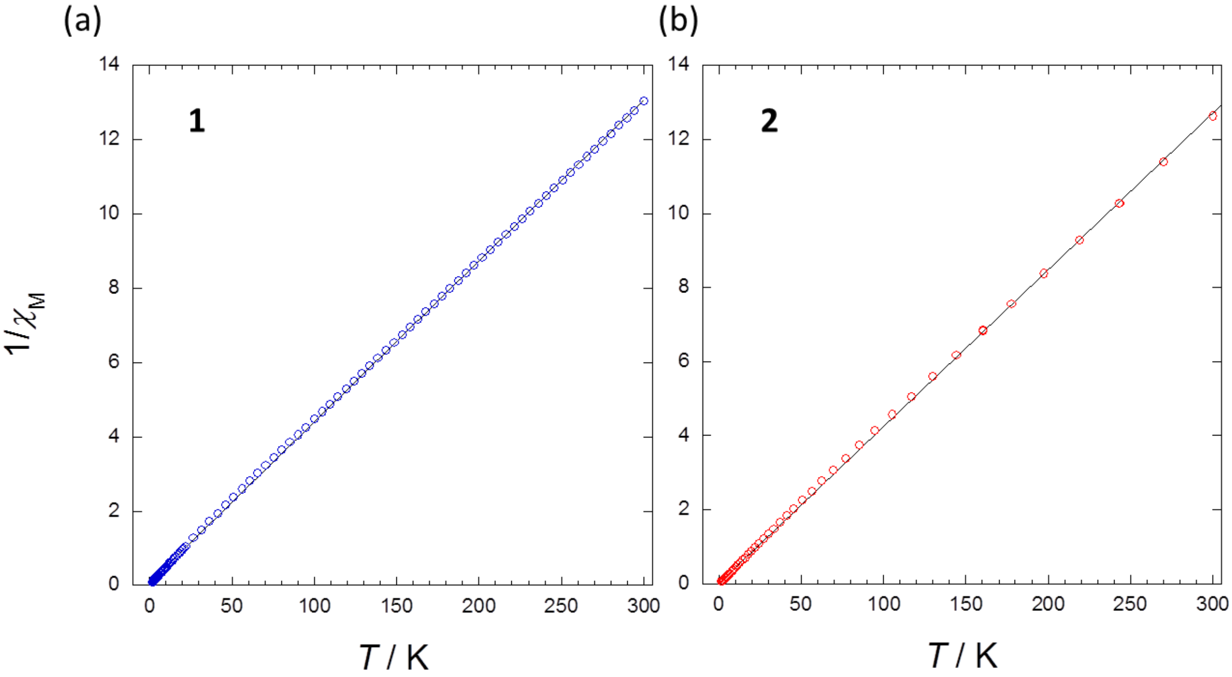

Fig. S7 $1/\chi_\mathrm{M}$ versus T plots for (a) **1** and (b) **2**. Black solid lines are linear fits of the data. The fitting parameters are listed in the main text.

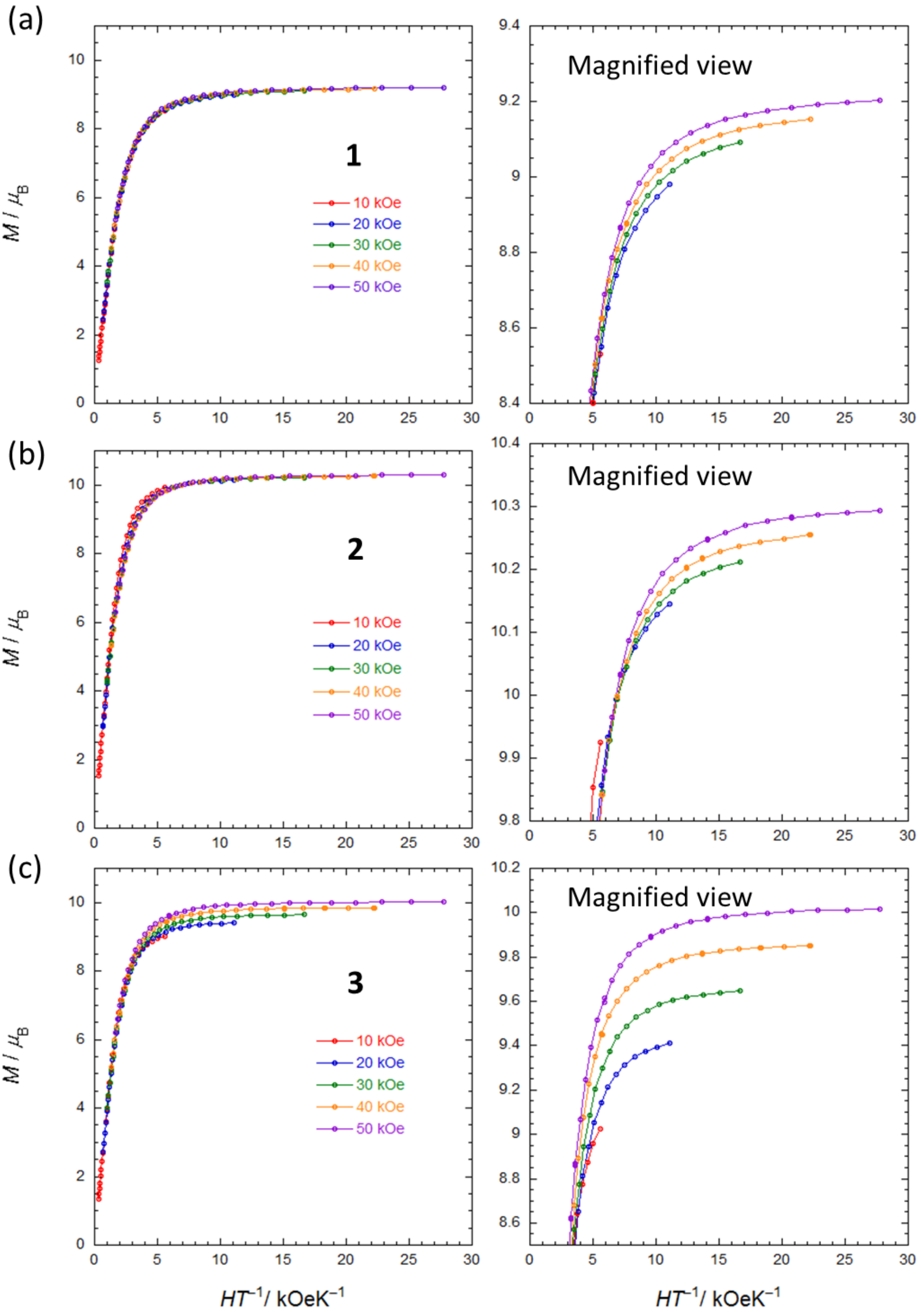

Fig. S8-1 Field dependence of the magnetization measured on powder samples of (a) **1**, (b) **2** and (c) **3**, corrected from 1.8 to 30 K. The solid lines are guides only.

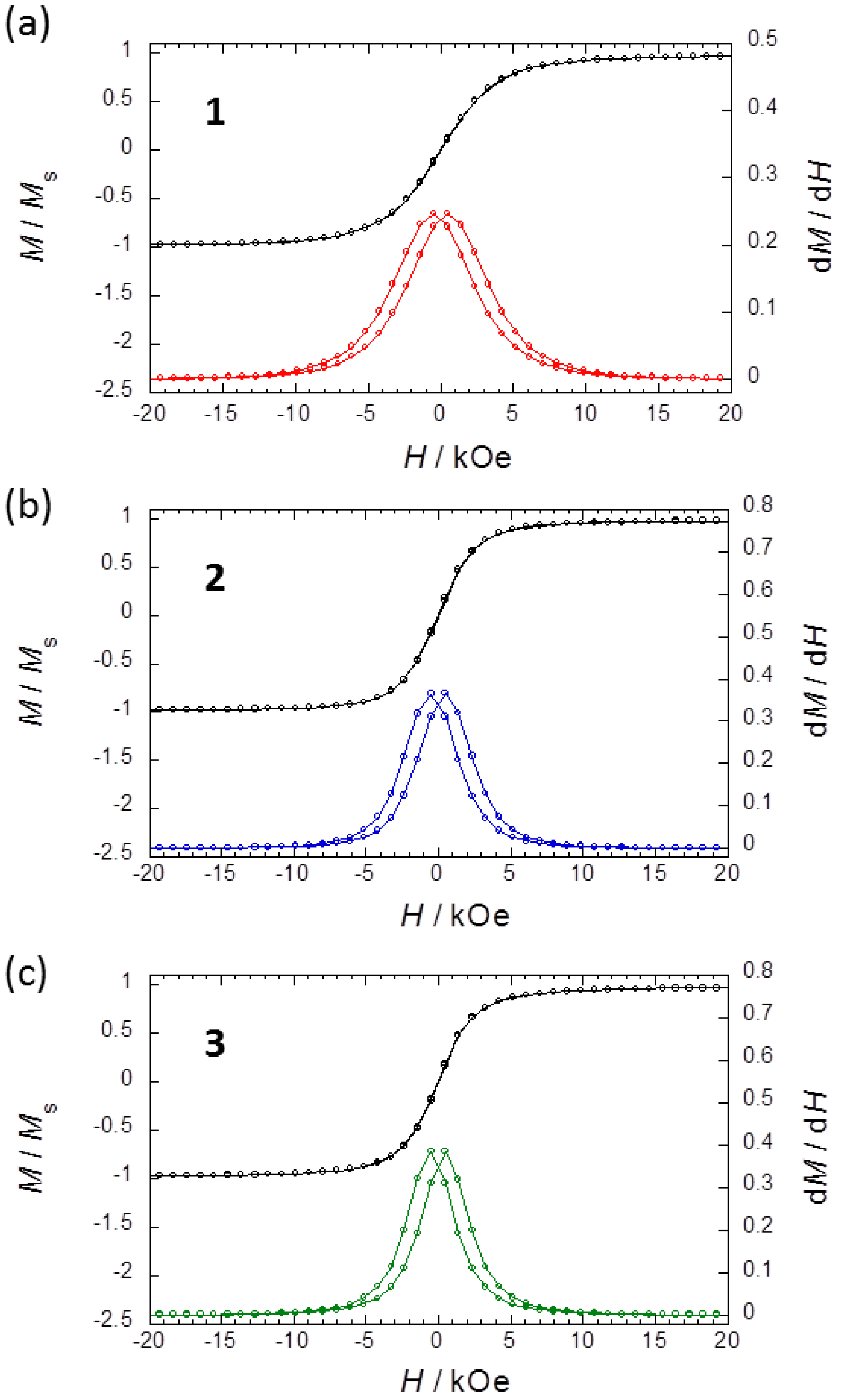

Fig. S8-2 Field dependence of the magnetization measured on powder samples of **1**–**3**, in which slight hystereses were observed at 1.8 K. The solid lines are guides only.

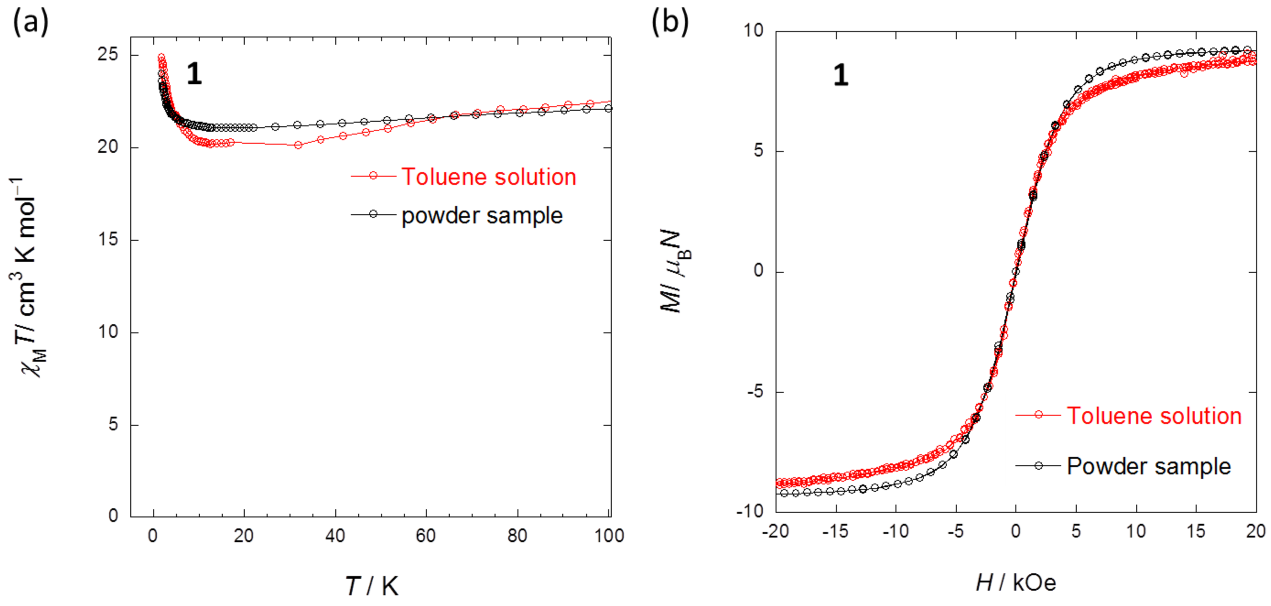

Fig. S9-1 (a) $\chi_M T$ versus T plots for **1**. The solution sample was prepare by mass ratio of **1** (5 mg) and toluene (1.8 mL). Open black circles are powder sample of **1**, and open red circles are solution sample of **1** (diluted sample). (b) The field dependence of the magnetization measured on powder (open black circles) and solution samples of **1** (open red circles). The solid lines are guides only.

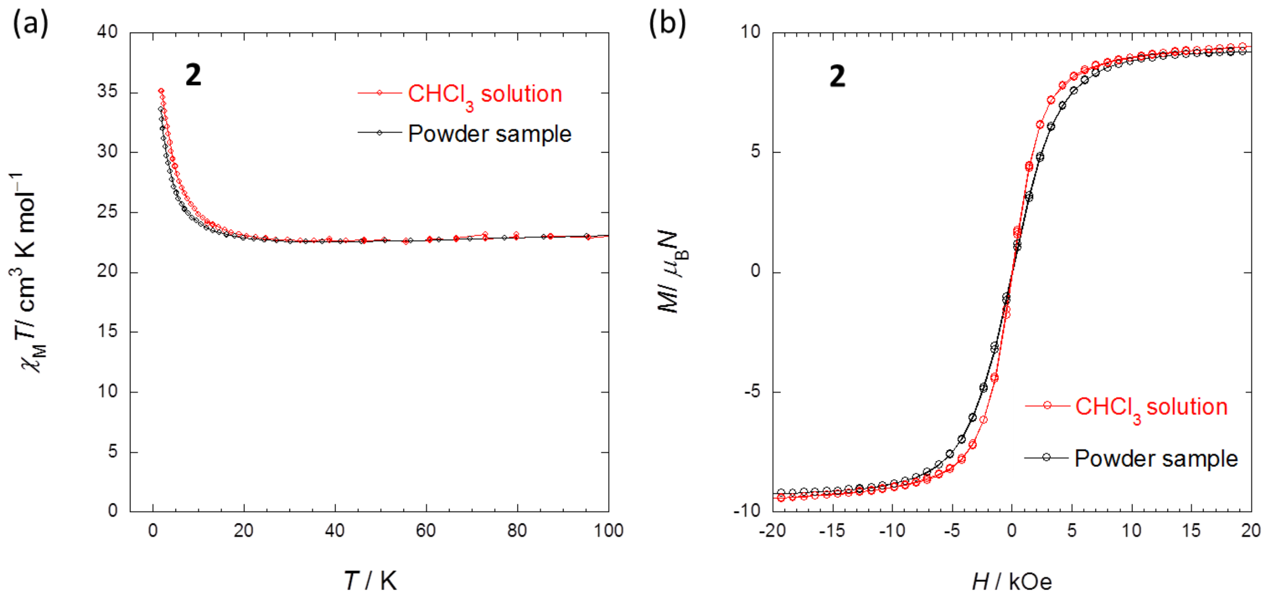

Fig. S9-2 (a) $\chi_M T$ versus T plots for **2**. Solution samples were prepared by using mass ratio of **2** (5 mg) and toluene (1.8 mL). Open black circles are powder sample of **2**, and open red circles are solution sample of **2** (diluted sample). (b) The field dependence of the magnetization was measured on powder (open black circles) and solution sample of **2** (open red circles). The solid lines are guides only.

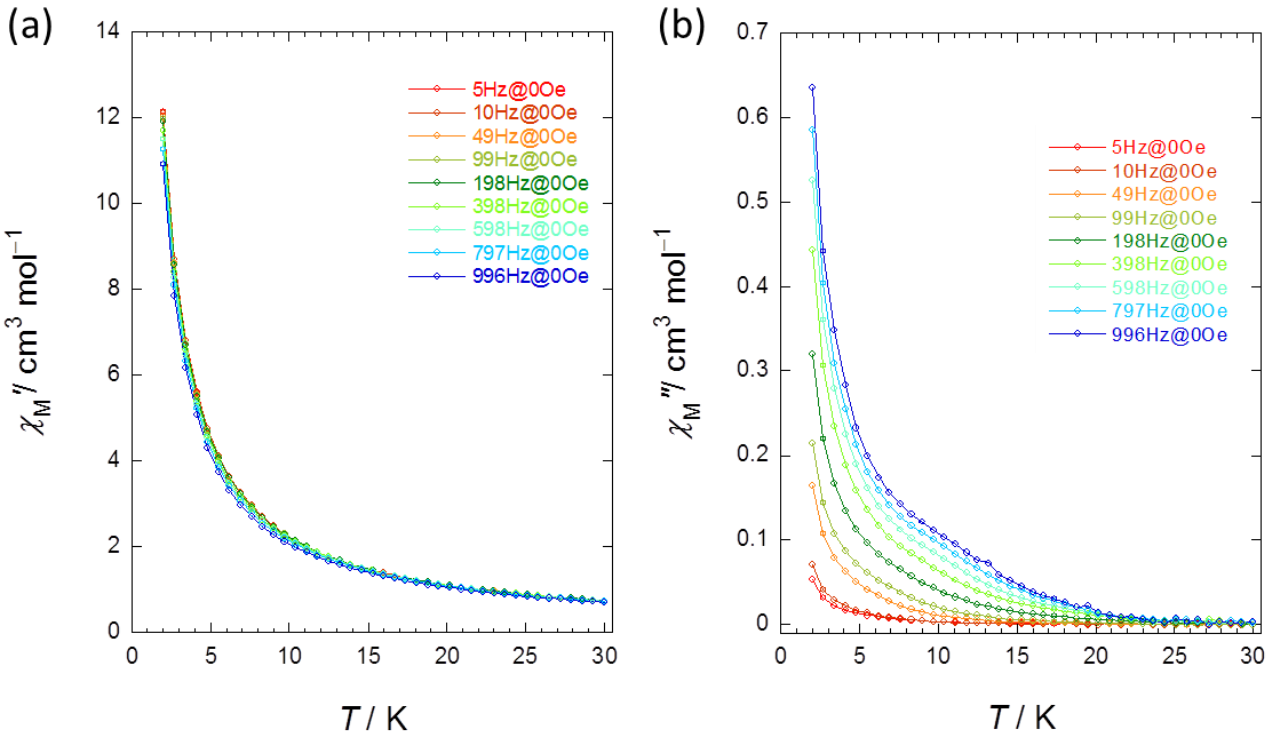

Fig. S10 Frequency (ν) and temperature (T) dependences of the (a) in-phase (χ_M') and (b) out-of-phase (χ_M'') ac magnetic susceptibilities of **1** in a zero dc field. The solid lines are guides only.

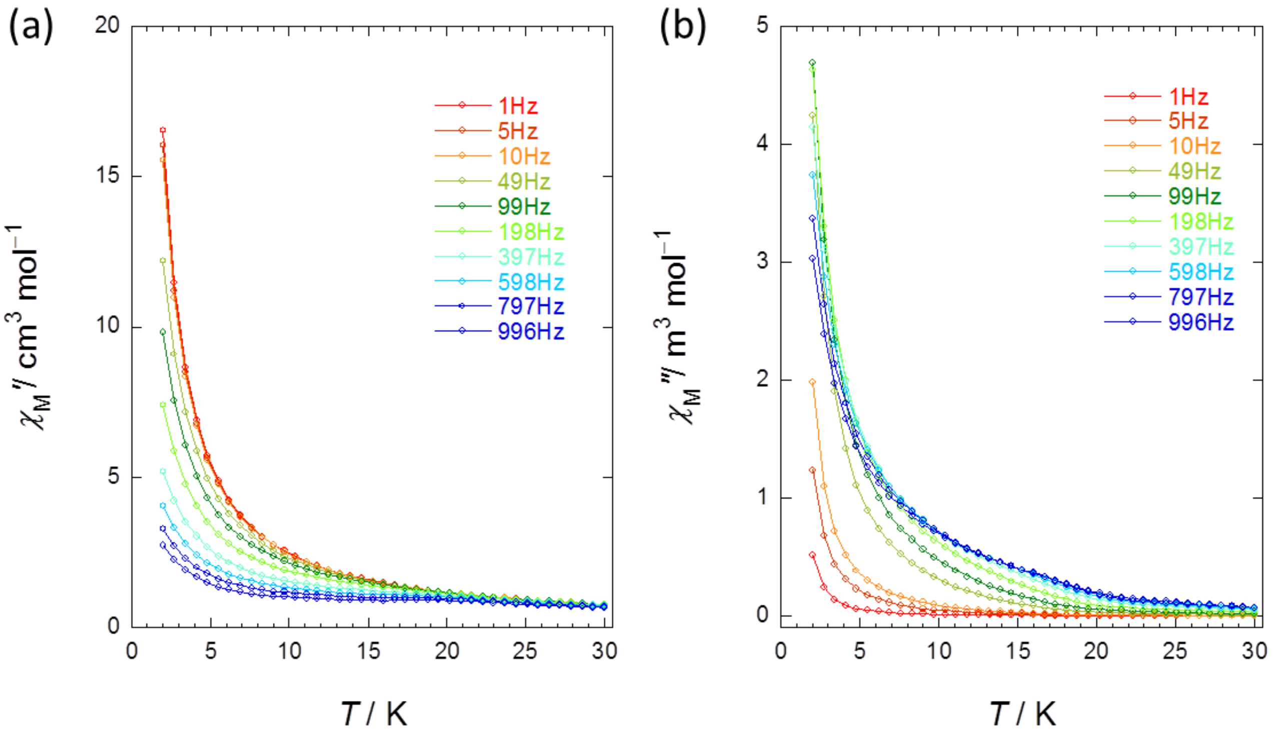

Fig. S11 Frequency (ν) and temperature (T) dependences of the (a) in-phase (χ_M') and (b) out-of-phase (χ_M'') ac magnetic susceptibilities of **2** at zero dc field. The solid lines are guides only.

The Kramers-Kronig equation[2–5]

$$\frac{\chi'}{\chi''} = \omega\tau \qquad \text{(eq. S1)}$$

$$\frac{\chi'}{\chi''} = \omega\tau_0 + exp\left(\frac{\Delta}{k_B T}\right) \qquad \text{(eq. S2)}$$

$$\ln\left(\frac{\chi'}{\chi''}\right) = \ln(\omega\tau_0) + \frac{\Delta}{k_B T} \qquad \text{(eq. S3)}$$

χ' : real part of ac magnetic susceptibility
χ'' : imaginary part of ac magnetic susceptibility
ω : the experimental ac field exciting frequency
Δ : the effective energy barrier
τ : the magnetic relaxation time
k_B: Boltzmann constant

Table S2. Selected values of Δ and τ_0 for **1**

ν / Hz	198	398	598	797	996
Δ/cm^{-1}	18.7	17.8	20.9	21.1	23.4
τ_0/s	1.35×10^{-6}	1.26×10^{-6}	8.1×10^{-7}	7.5×10^{-7}	5.7×10^{-7}

Table S3. Selected values of Δ and τ_0 for **2**

ν / Hz	198	398	598	797	996
Δ/cm^{-1}	37.8	38.0	37.8	36.4	36.0
τ_0/s	4.52×10^{-6}	3.48×10^{-6}	2.92×10^{-6}	2.82×10^{-6}	2.61×10^{-6}

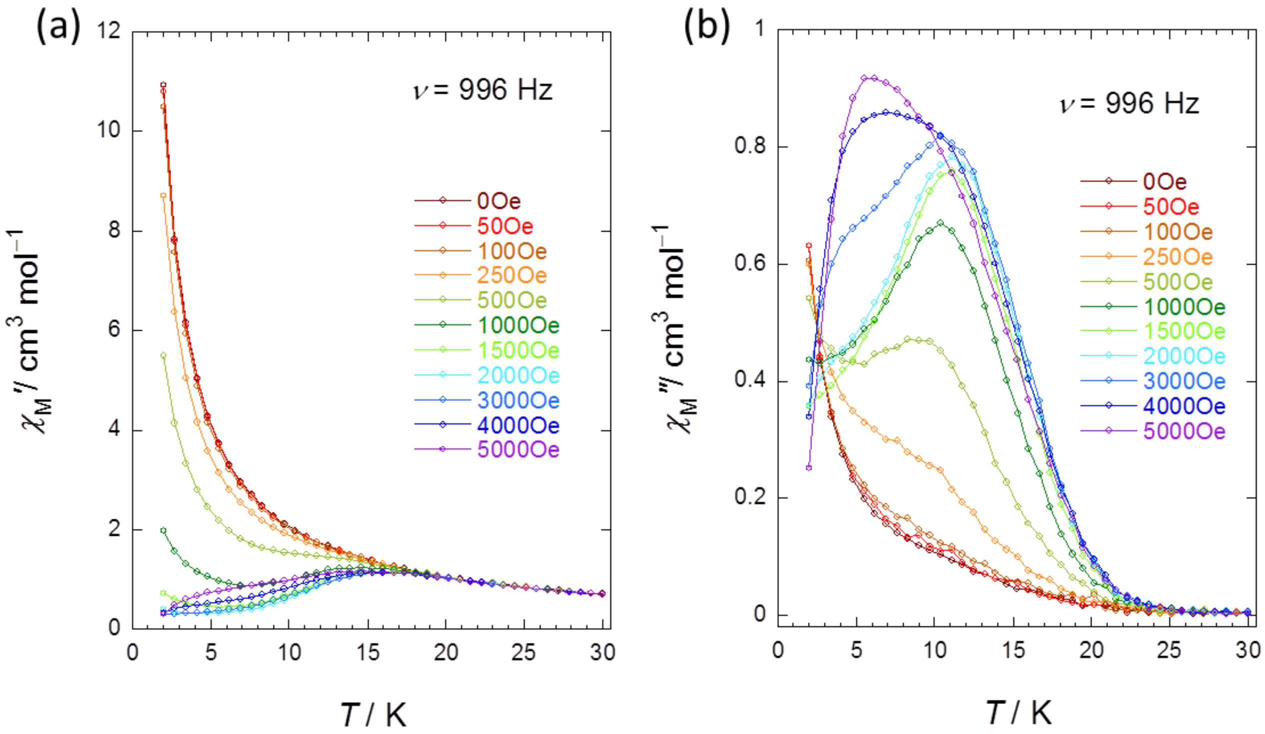

Fig. S12 Frequency (*ν*) and temperature (*T*) dependences of the (a) in-phase (χ_M') and (b) out-of-phase (χ_M'') ac magnetic susceptibilities of **1** at 996 Hz in several dc magnetic fields. The solid lines are guides only.

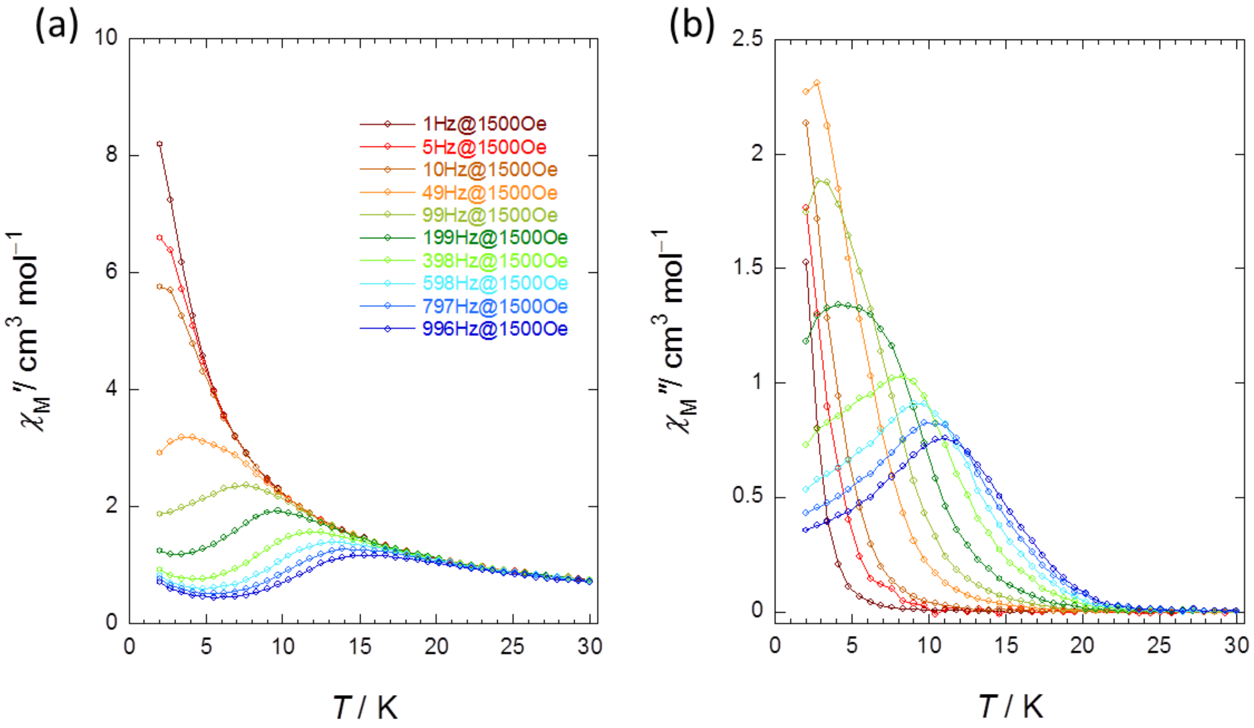

Fig. S13-1 Frequency (*ν*) and temperature (*T*) dependences of the (a) in-phase (χ_M') and (b) out-of-phase (χ_M'') ac magnetic susceptibilities of **1** at 1500 Oe. The solid lines are guides only.

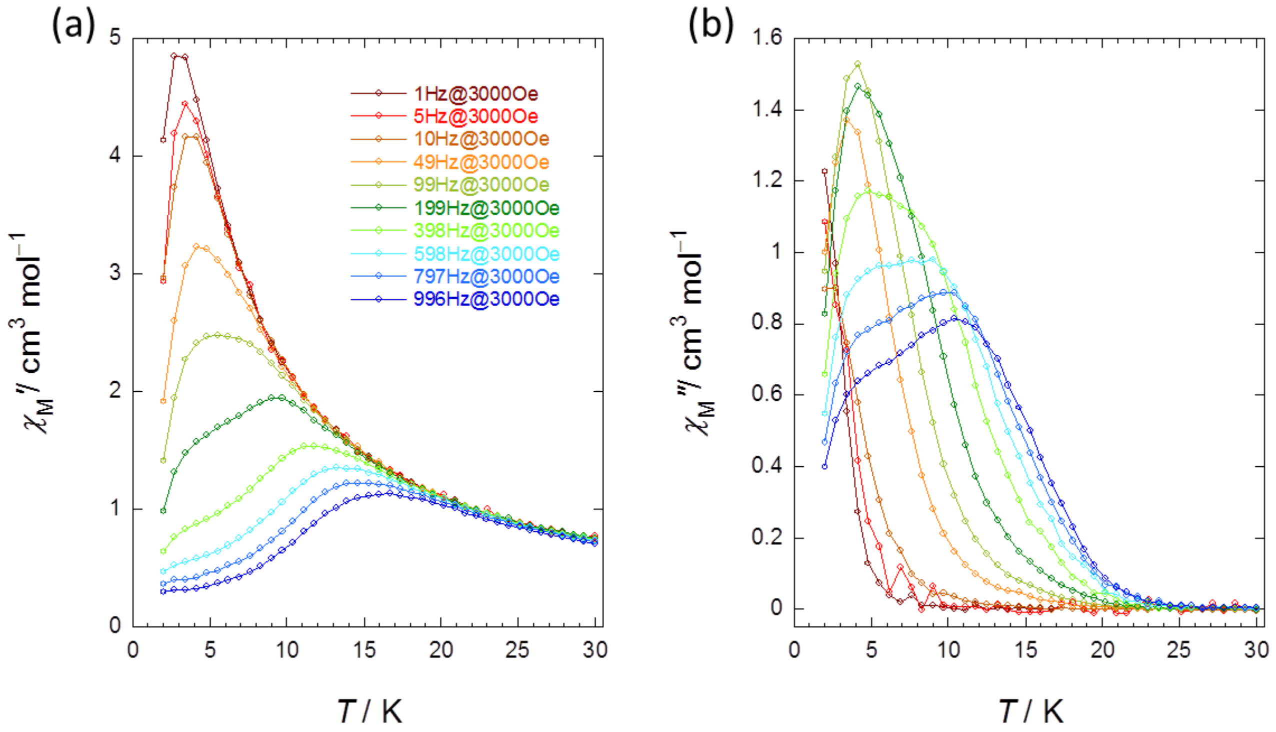

Fig. S13-2 Frequency (ν) and temperature (T) dependences of the (a) in-phase (χ_M') and (b) out-of-phase (χ_M'') ac magnetic susceptibilities of **1** at 3000 Oe. The solid lines are guides only.

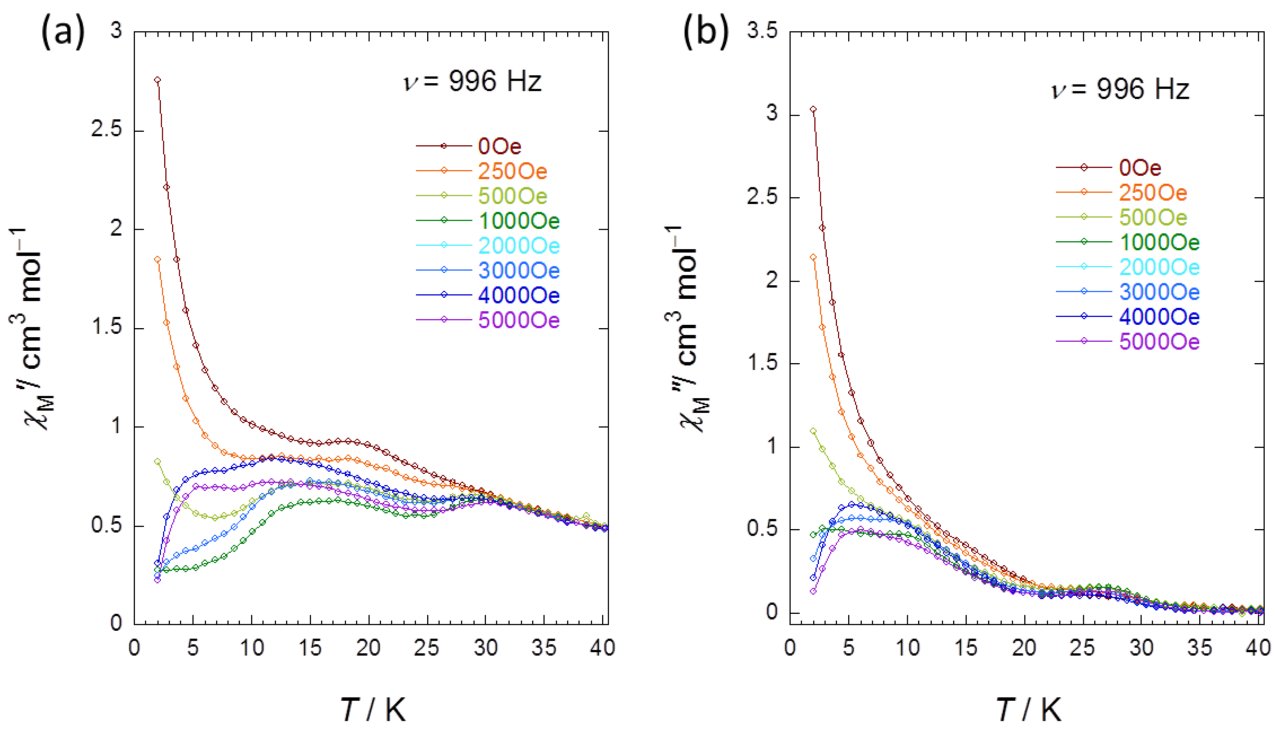

Fig. S14 Frequency (ν) and temperature (T) dependences of the (a) in-phase (χ_M') and (b) out-of-phase (χ_M'') ac magnetic susceptibilities of **2** at 996 Hz in several dc magnetic fields. The solid lines are guides only.

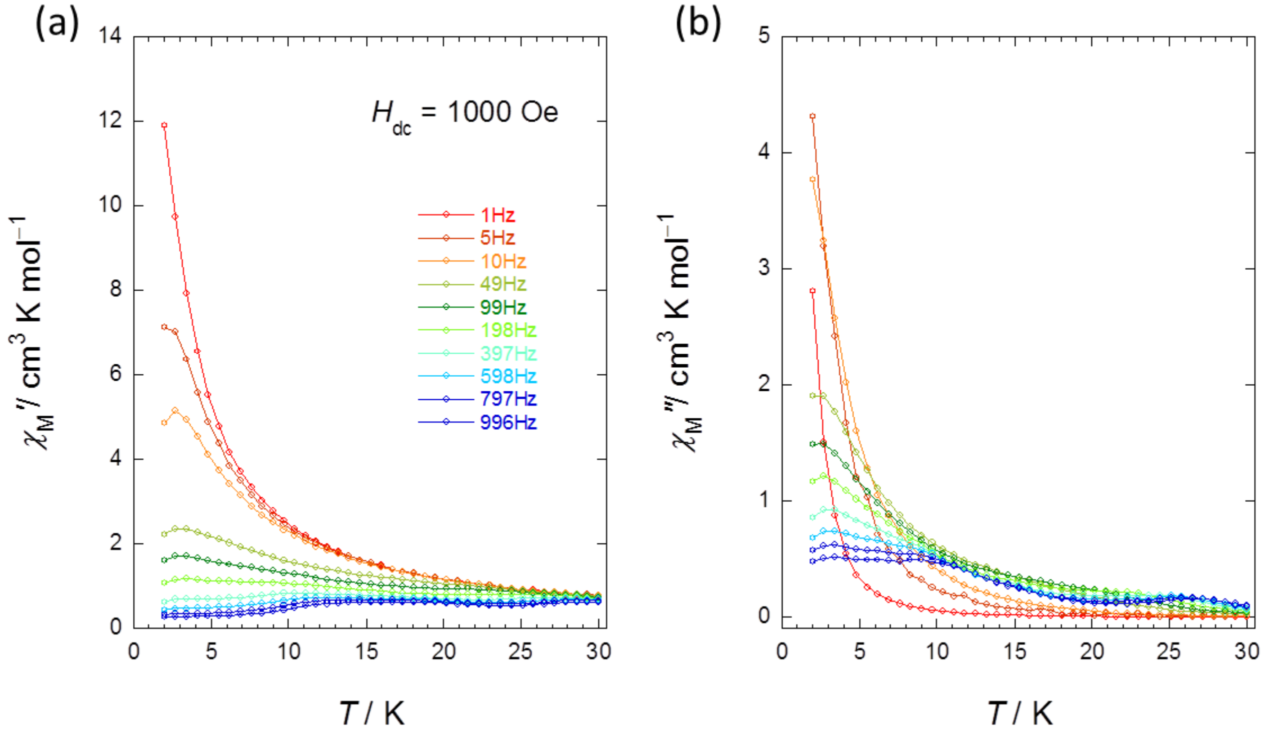

Fig. S15 Frequency (ν) and temperature (T) dependences of the (a) in-phase (χ_M') and (b) out-of-phase (χ_M'') ac magnetic susceptibilities of **2** at 1000 Oe. The solid lines are guides only.

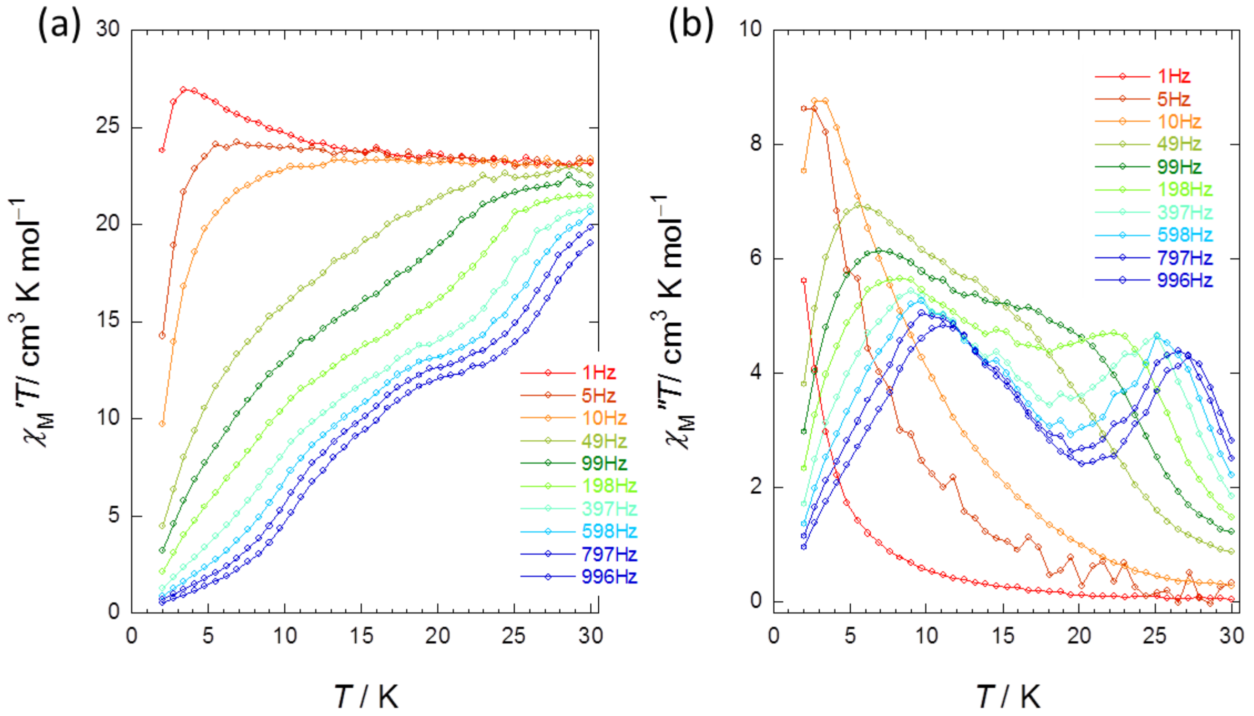

Fig. S16 Frequency (ν) and temperature (T) dependences of the ac magnetic susceptibilities of **2** at 1000 Oe: (a) $\chi_M'T$ and (b) $\chi_M''T$. The solid lines are guides only.

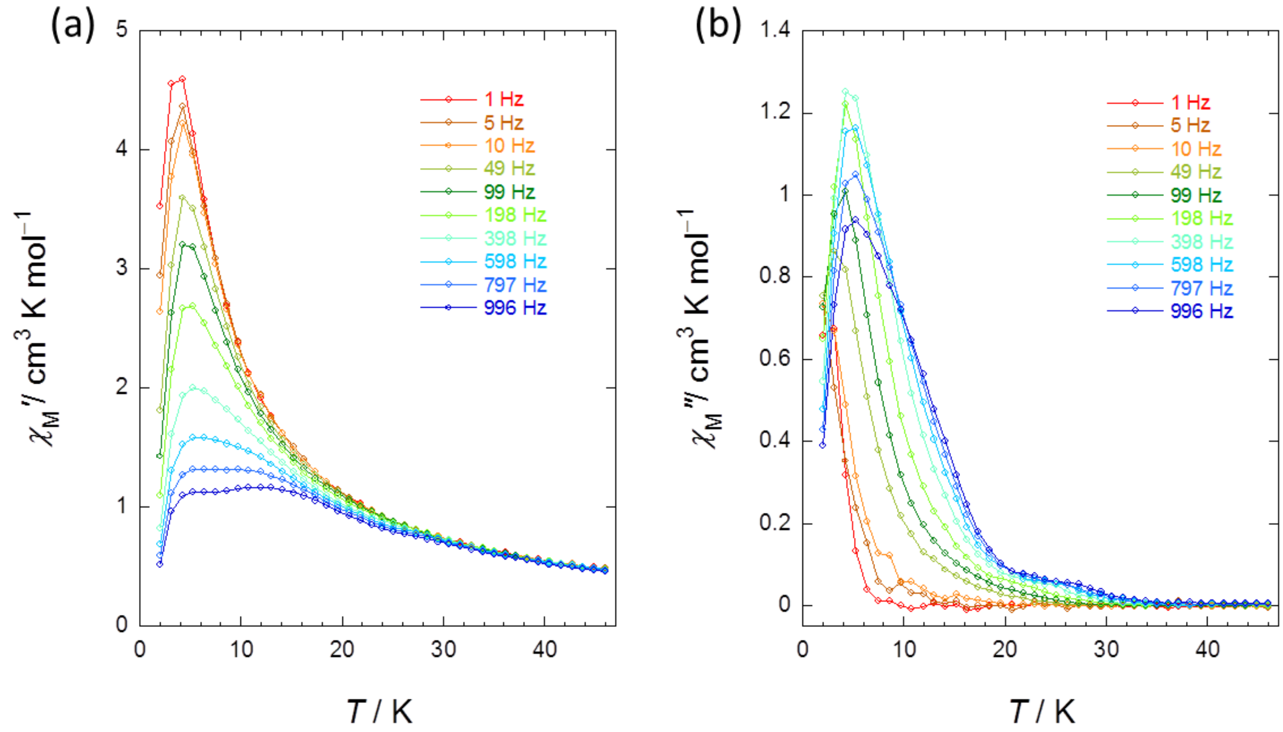

Fig. S17 Frequency (ν) and temperature (T) dependences of the (a) in-phase (χ_M') and (b) out-of-phase (χ_M'') ac magnetic susceptibilities of **2** at 3000 Oe. The solid lines are guides only.

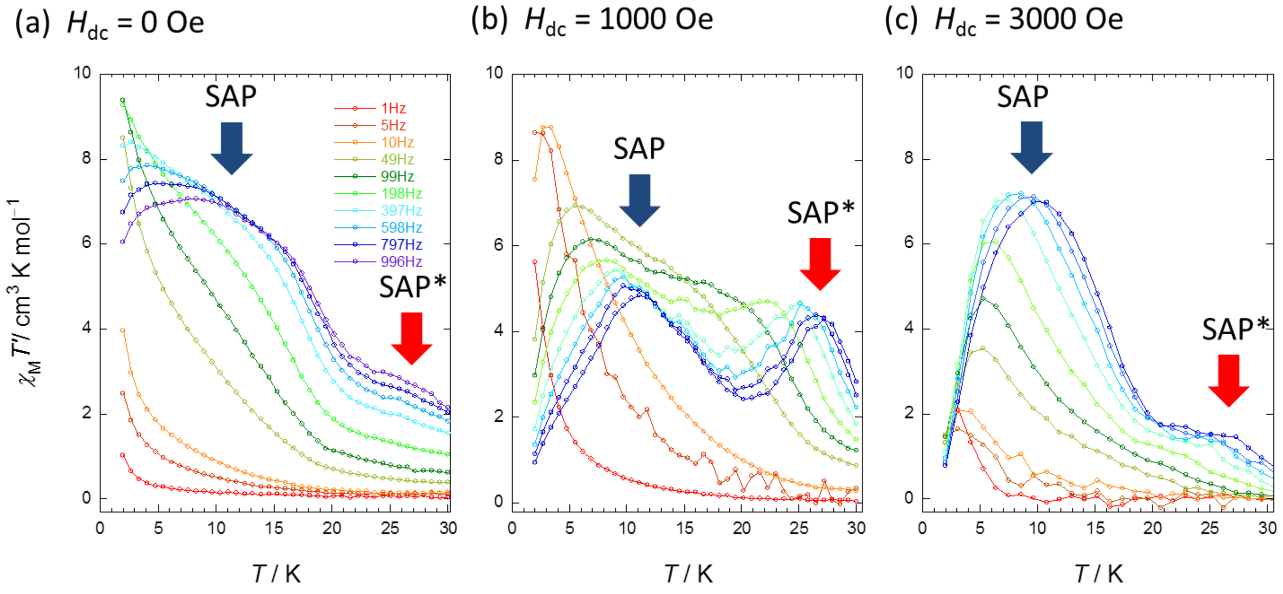
(a) H_{dc} = 0 Oe
(b) H_{dc} = 1000 Oe
(c) H_{dc} = 3000 Oe

Fig. S18 Frequency (ν) and temperature (T) dependences of χ_M'' of **2** (SAP = Site A, SAP* = Site B). (a) H_{dc} = 0, (b) 1000, and (c) 3000 Oe. The solid lines are guides only.

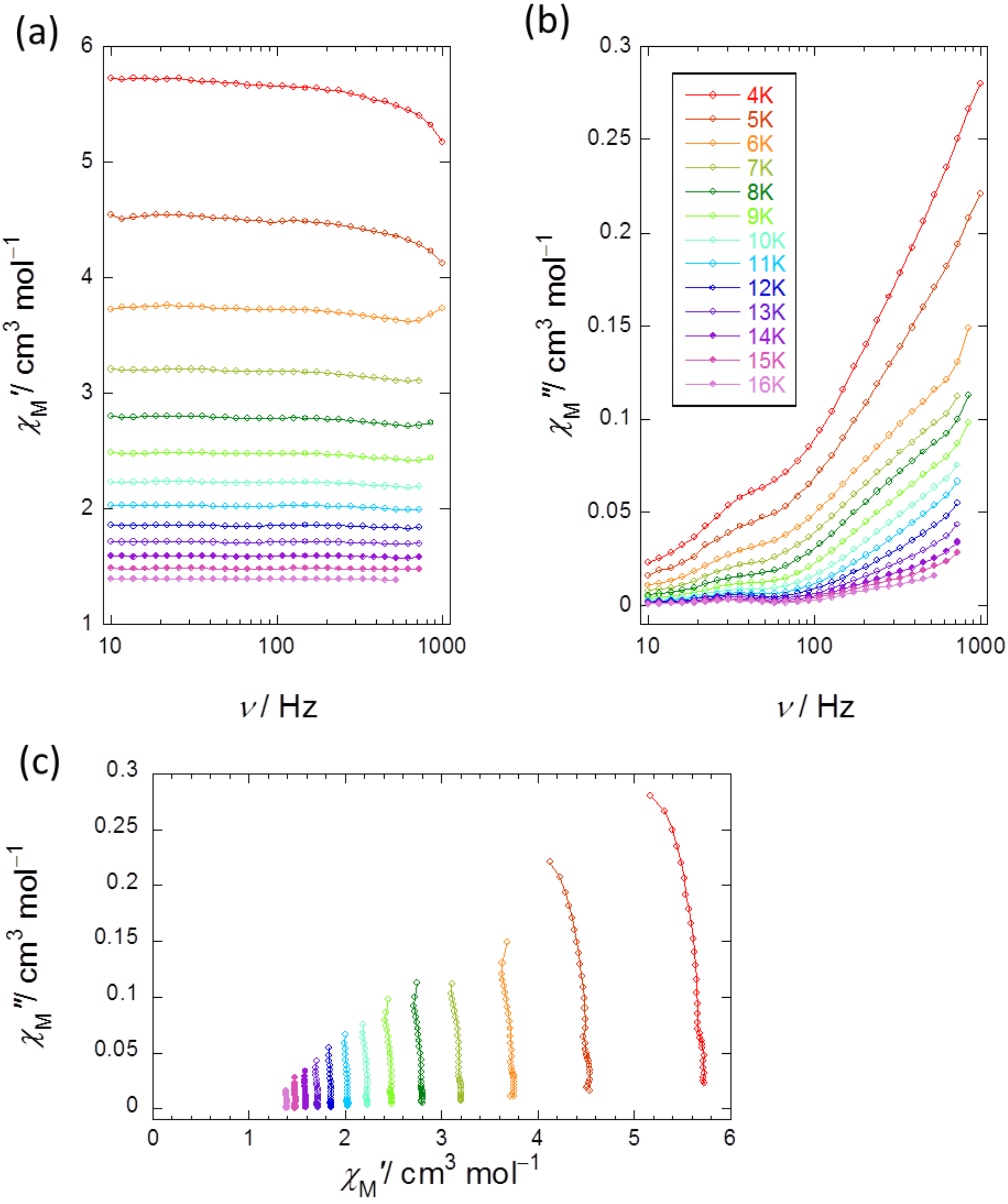

Fig. S19 Frequency (ν) dependence of (a) the real (χ_M') and (b) imaginary (χ_M'') parts of the ac susceptibilities of **1** measured between 4 and 16 K in an H_{dc} of zero. (c) Argand plot of **1**. The solid lines are guides only.

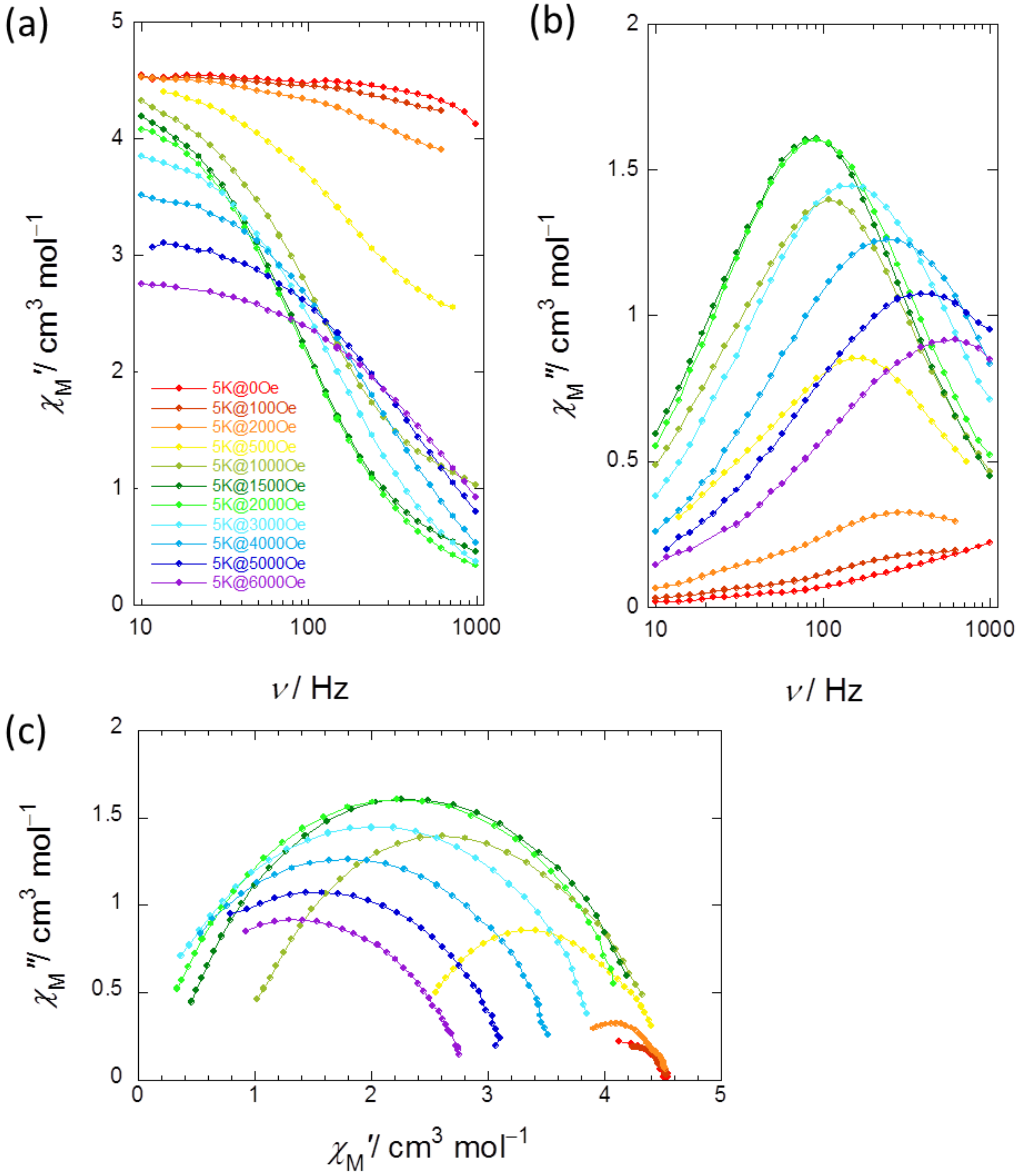

Fig. S20 Frequency (ν) dependence of (a) the real (χ_M') and (b) imaginary (χ_M'') parts of the ac susceptibilities of **1** measured between 0 and 6000 Oe at 5 K. (c) Argand plot of **1** measured between 0 and 6000 Oe at 5 K. The solid lines are guides only.

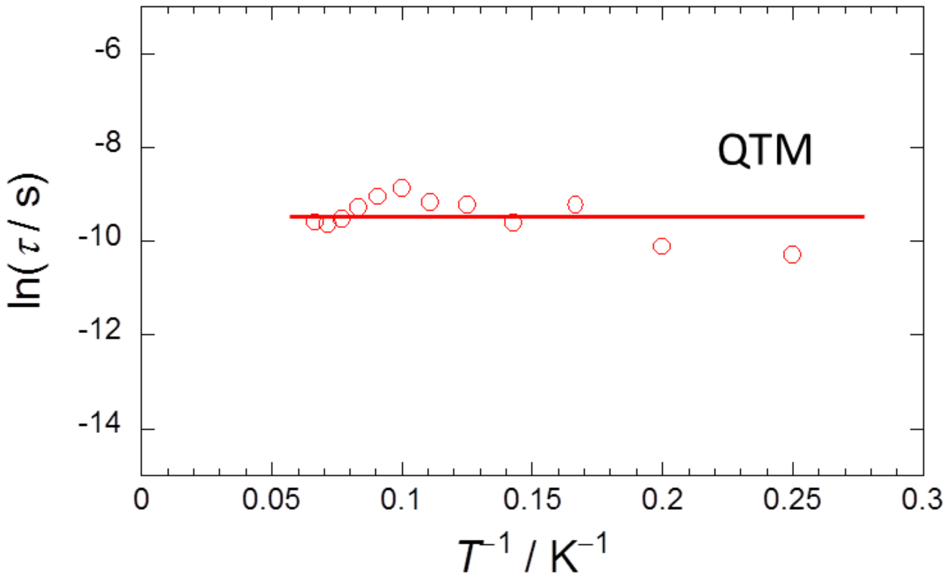

Fig. S21 Arrhenius plots for **1** in a zero H_{dc}. Estimates of τ from Fig. S20b (see main text). The solid line is guide only.

Table S4. τ values at 5 K for **1–3** in several H_{dc}

Complexes	τ/s at 5 K	H_{dc}/ Oe
[(TTP)Tb(Pc)Tb(TTP)] (**1**)	4.1×10^{-5}	0
	2.0×10^{-3}	1500
[(Pc)Tb(Pc)Tb(TTP)] (**2**)	5.6×10^{-4}	0
	5.2×10^{-4} (τ_1)	1000
	1.2×10^{-2} (τ_2)	1000
	4.0×10^{-4} (τ_1)	3000
	2.4×10^{-3} (τ_2)	3000
[(obPc)Tb(obPc)Tb(obPc)] (**3**)	1.8×10^{-2}	0
	4.8×10^{-3} (τ_1)	3000
	4.5×10^{-2} (τ_2)	3000

The experimental data of **3** from ref. 7e (see main text).

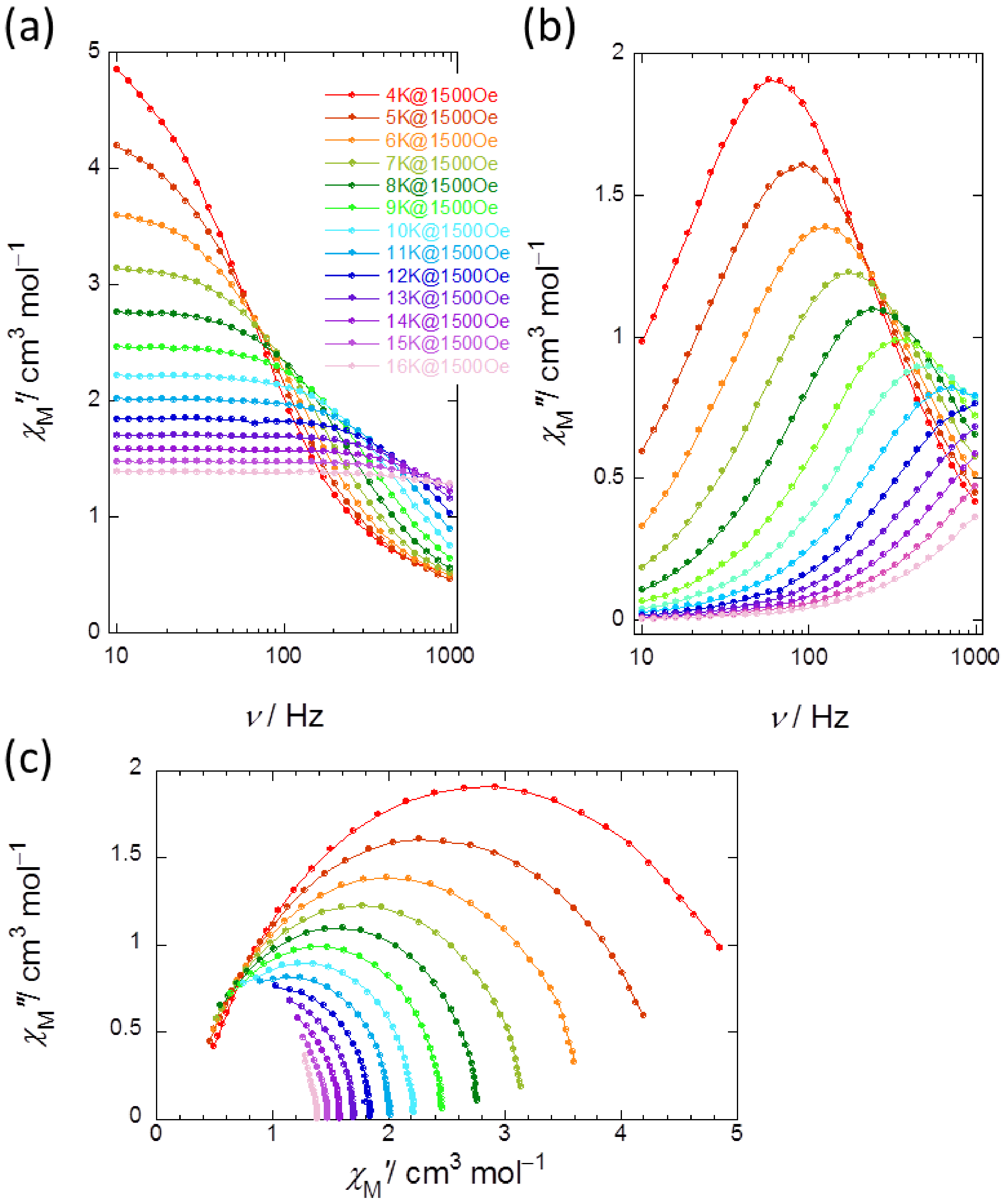

Fig. S22 Frequency (ν) dependence of (a) the real (χ_M') and (b) imaginary (χ_M'') parts of the ac susceptibilities of **1** measured between 4 and 16 K in an H_{dc} of 1500 Oe. (c) Argand plot for **1**. The solid lines are guides only.

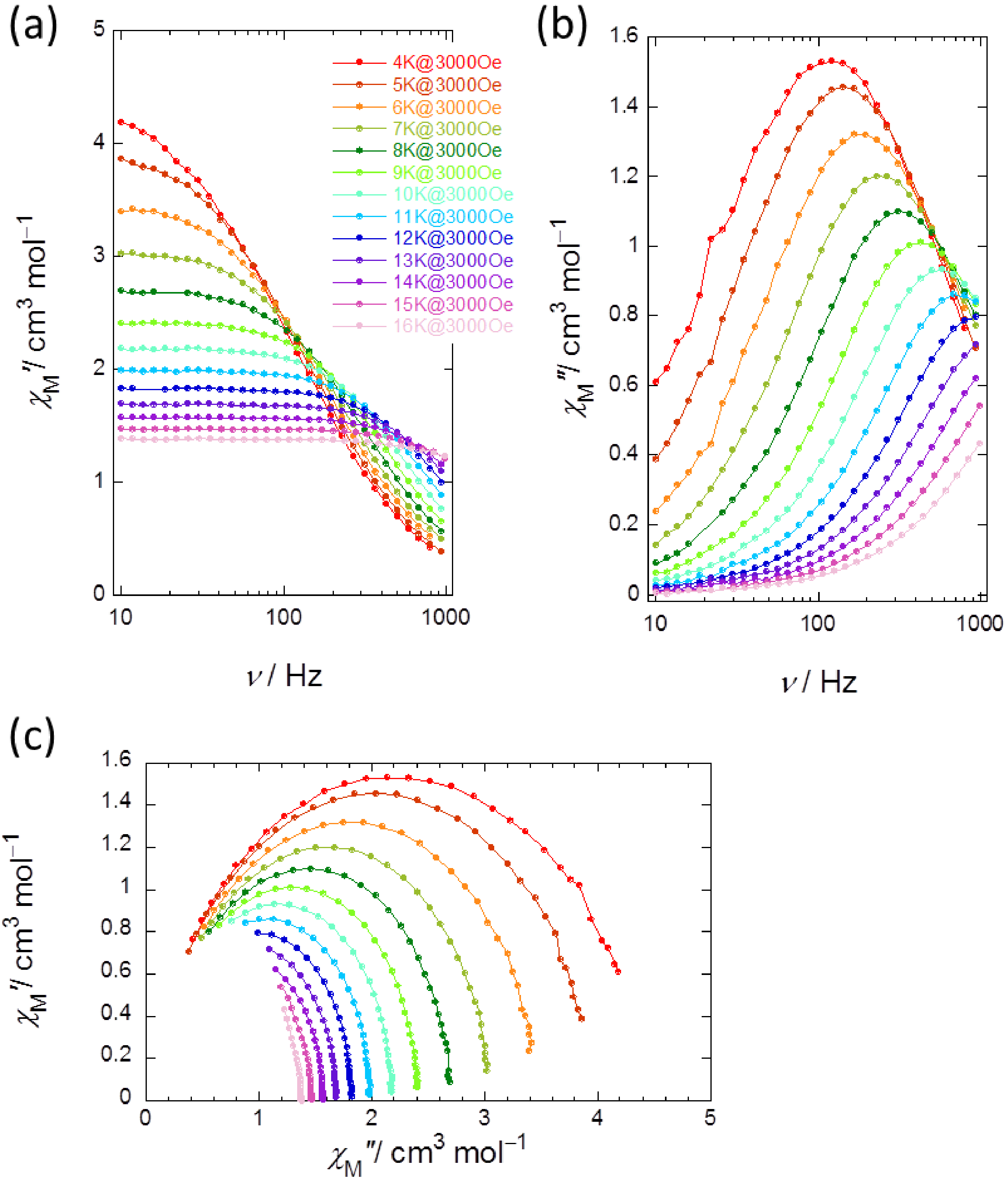

Fig. S23 Frequency (ν) dependence of (a) the real (χ_M') and (b) imaginary (χ_M'') parts of the ac susceptibilities of **1** measured between 4 and 16 K in a H_{dc} of 3000 Oe. (c) Argand plot for **1**. The solid lines are guides only.

The generalized Debye model (eq. S4)[6]

The real (χ_M') and imaginary parts (χ_M'') are given by eqs. S5 and S6, respectively.

$$\chi_{total}(\omega) = \chi_S + \frac{\chi_T - \chi_S}{1 + (i\omega\tau)^{1-\alpha}} \quad \text{(eq. S4)}$$

$$\chi'(\omega) = \chi_S + (\chi_T - \chi_S)\frac{1 + (\omega\tau)^{1-\alpha}\sin(\pi\alpha/2)}{1 + 2(\omega\tau)^{1-\alpha}\sin(\pi\alpha/2) + (\omega\tau)^{2-2\alpha}} \quad \text{(eq. S5)}$$

$$\chi''(\omega) = (\chi_T - \chi_S)\frac{(\omega\tau)^{1-\alpha}\cos(\pi\alpha/2)}{1 + 2(\omega\tau)^{1-\alpha}\sin(\pi\alpha/2) + (\omega\tau)^{2-2\alpha}} \quad \text{(eq. S6)}$$

The Arrhenius equation

From the ν dependence of T_B at each T, it is possible to estimate Δ and τ_0, which is the average τ in response to thermal fluctuation, from the generalized Debye model by using the Arrhenius equation (eq. S7). This linear relation between ln(τ) and T^{-1} indicates that the Orbach process (spin-phonon interactions), which approximately correspond to the Δ for thermal relaxation of the reversal of the magnetic moment, is dominant in high-T ranges (see main text).

$$\tau = \tau_0 exp(\Delta E/k_B T) \quad \text{(eq. S7-1)}$$

$$\ln(\tau) = ln(\tau_0) + \Delta E/k_B T \quad \text{(eq. S7-2)}$$

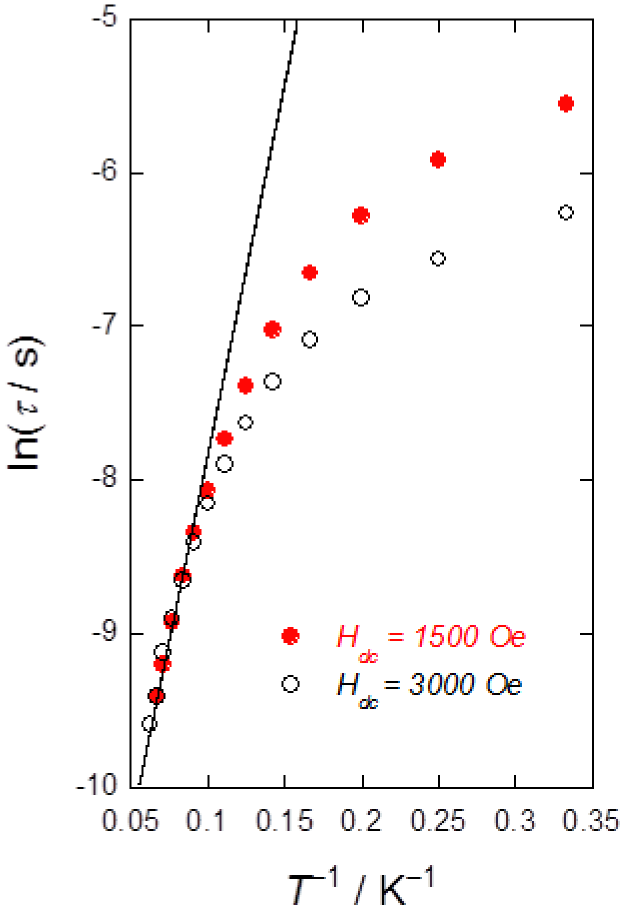

Fig. S24 An Arrhenius plot of **1**, where the τ were obtained from χ_M'' versus ν plots at T between 4 and 16 K in an H_{dc} of 1500 (Fig. S22b) and 3000 Oe (Fig. S23b). The solid lines were fitted using an Arrhenius law. The fitting parameters are listed in the main text.

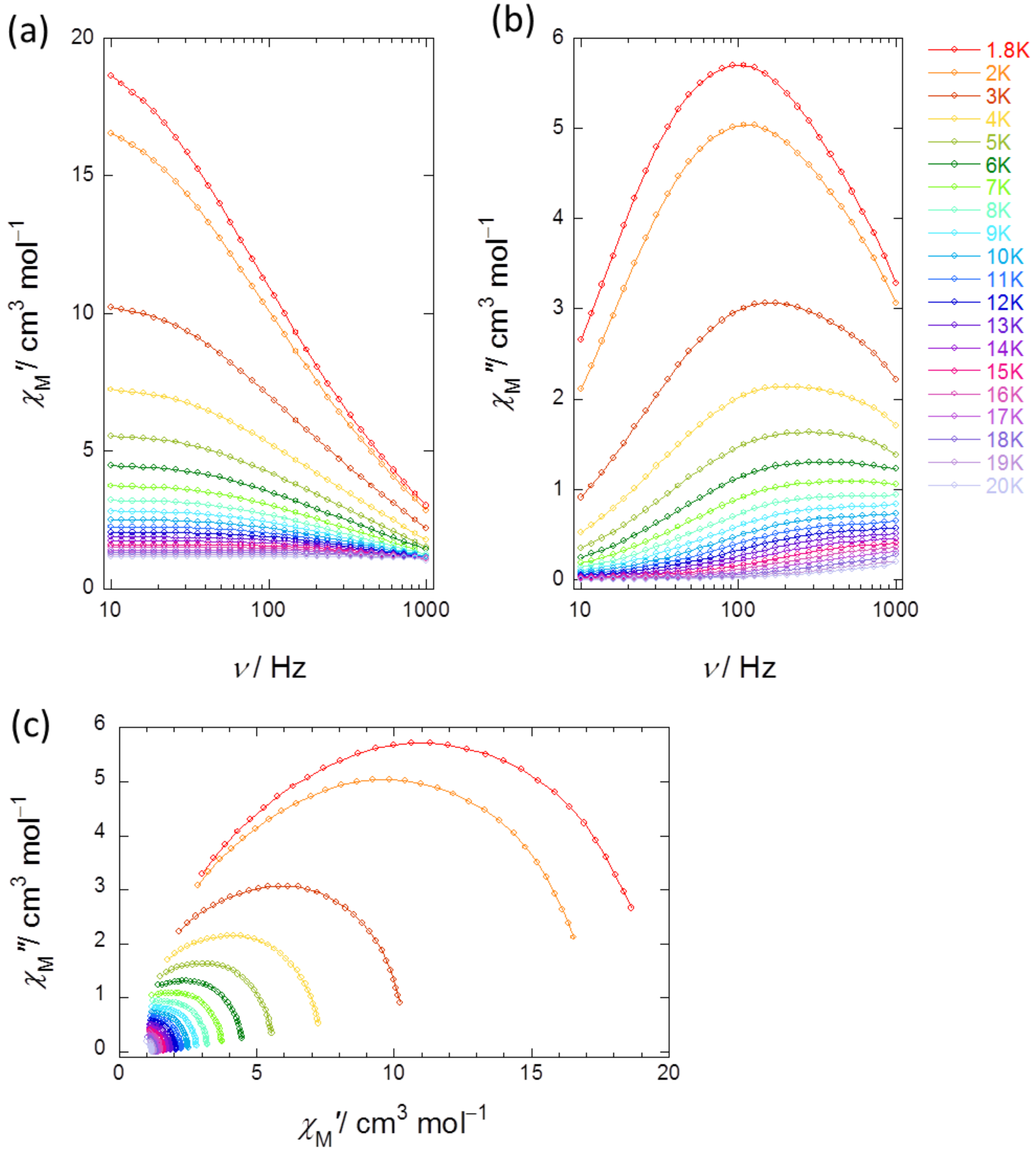

Fig. S25 Frequency (ν) dependence of (a) the real (χ_M') and (b) imaginary (χ_M'') parts of the ac susceptibilities of **2** measured between 1.8 and 20 K in an H_{dc} of zero. (c) Argand plot for **2**. The solid lines are guides only.

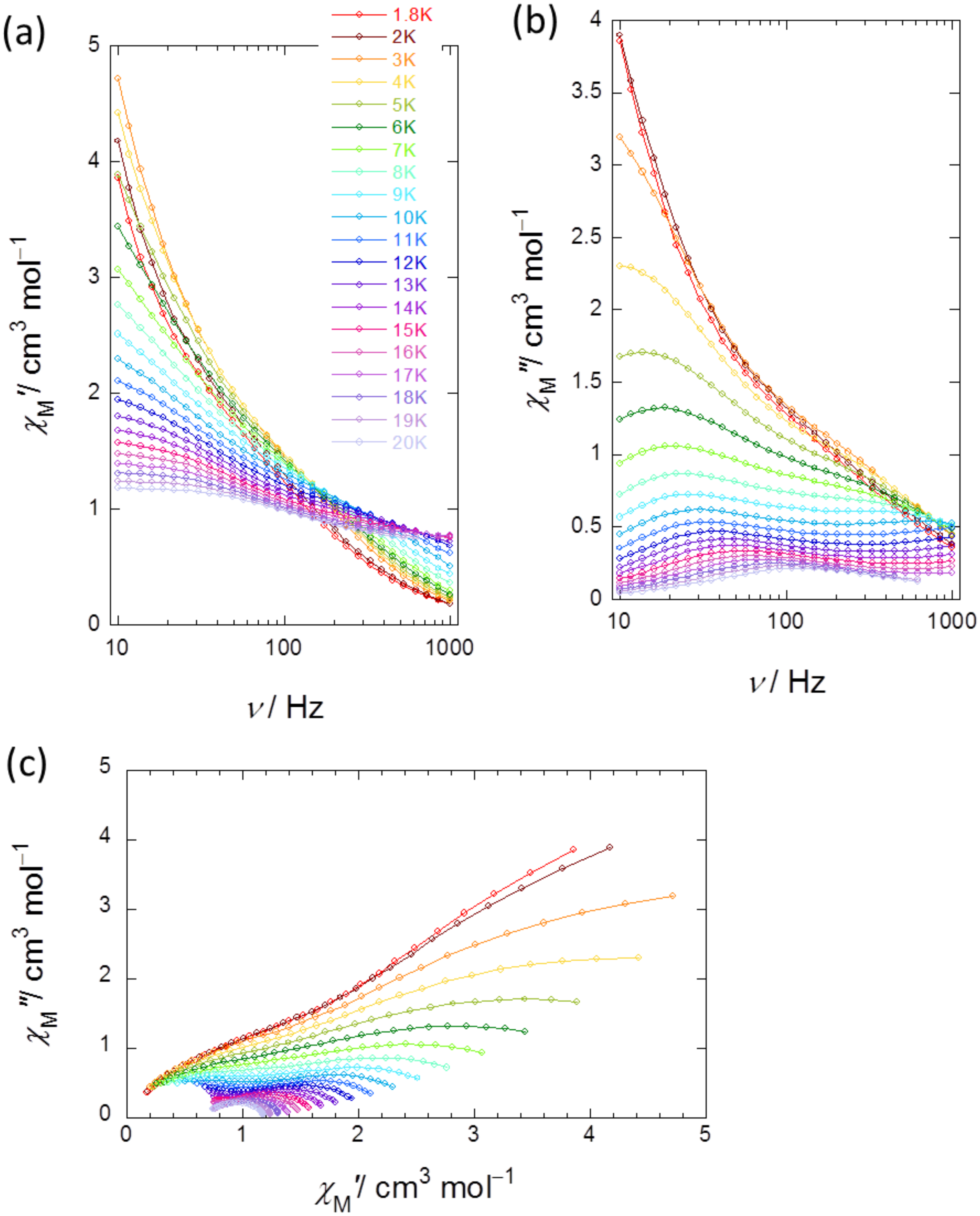

Fig. S26 Frequency (ν) dependence of (a) the real (χ_M') and (b) imaginary (χ_M'') parts of the ac susceptibilities of **2** measured between 1.8 and 20 K in an H_{dc} of 1000 Oe. (c) Argand plot for **2**. The solid lines are guides only.

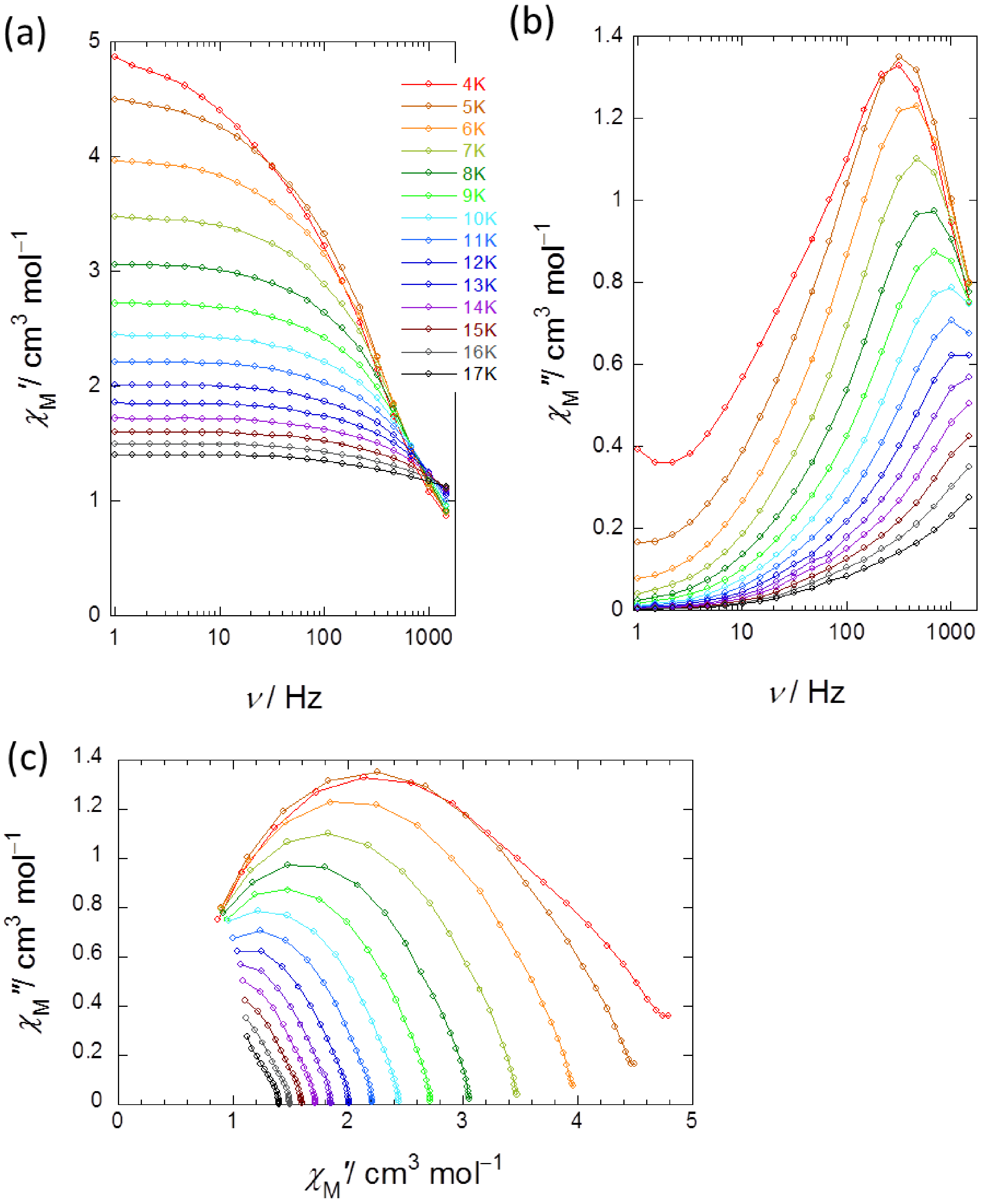

Fig. S27 Frequency (ν) dependence of (a) the real (χ_M') and (b) imaginary (χ_M'') parts of the ac susceptibilities of **2** measured between 1.8 and 20 K in a H_{dc} of 3000 Oe. (c) Argand plot for **2**. The solid lines are guides only.

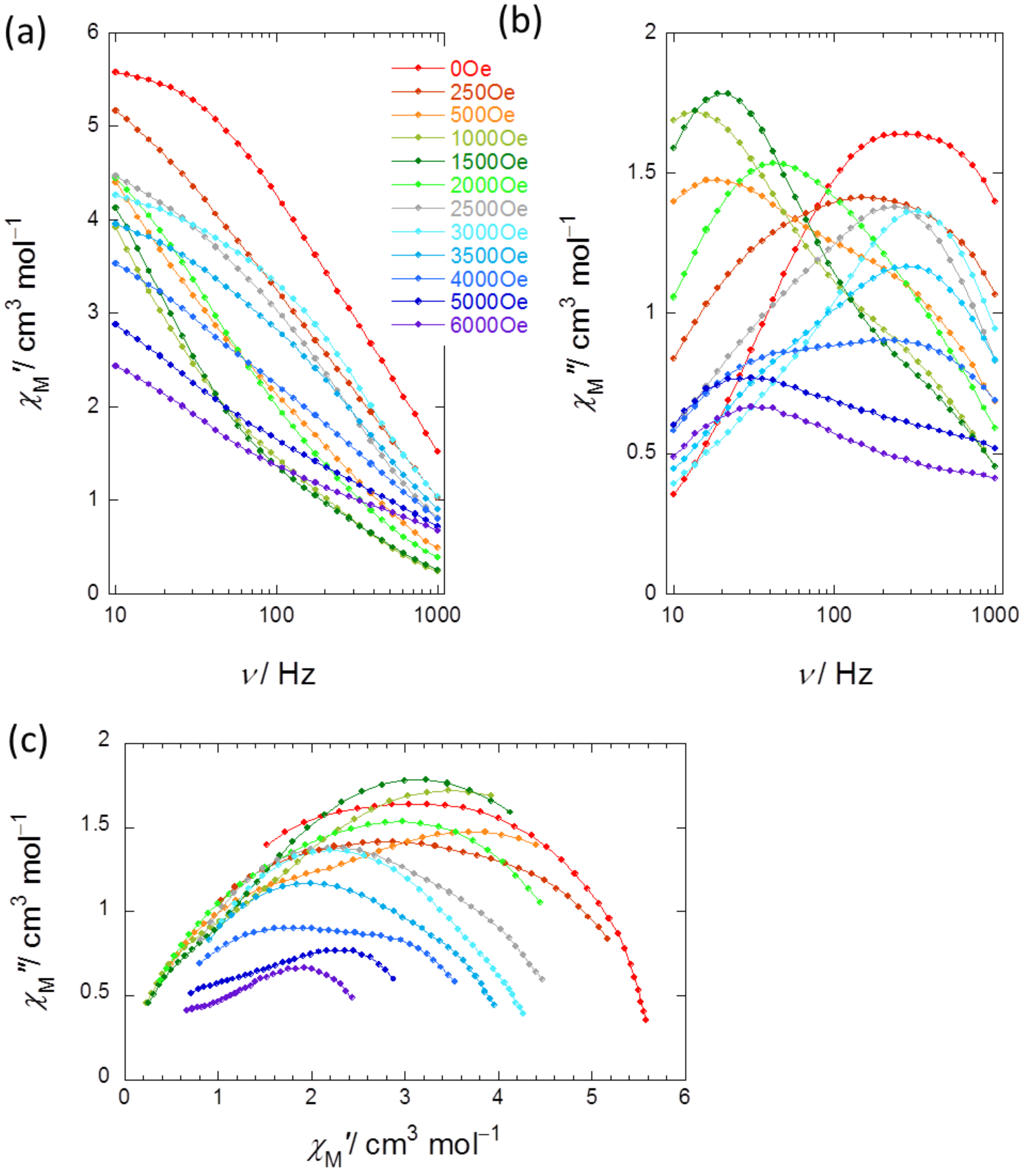

Fig. S28 Frequency (ν) dependence of (a) the real (χ_M') and (b) imaginary (χ_M'') parts of the ac susceptibilities of **2** measured between 0 and 6000 Oe at 5 K. Argand plot for **2** measured between 0 and 6000 Oe at 5 K. The solid lines are guides only.

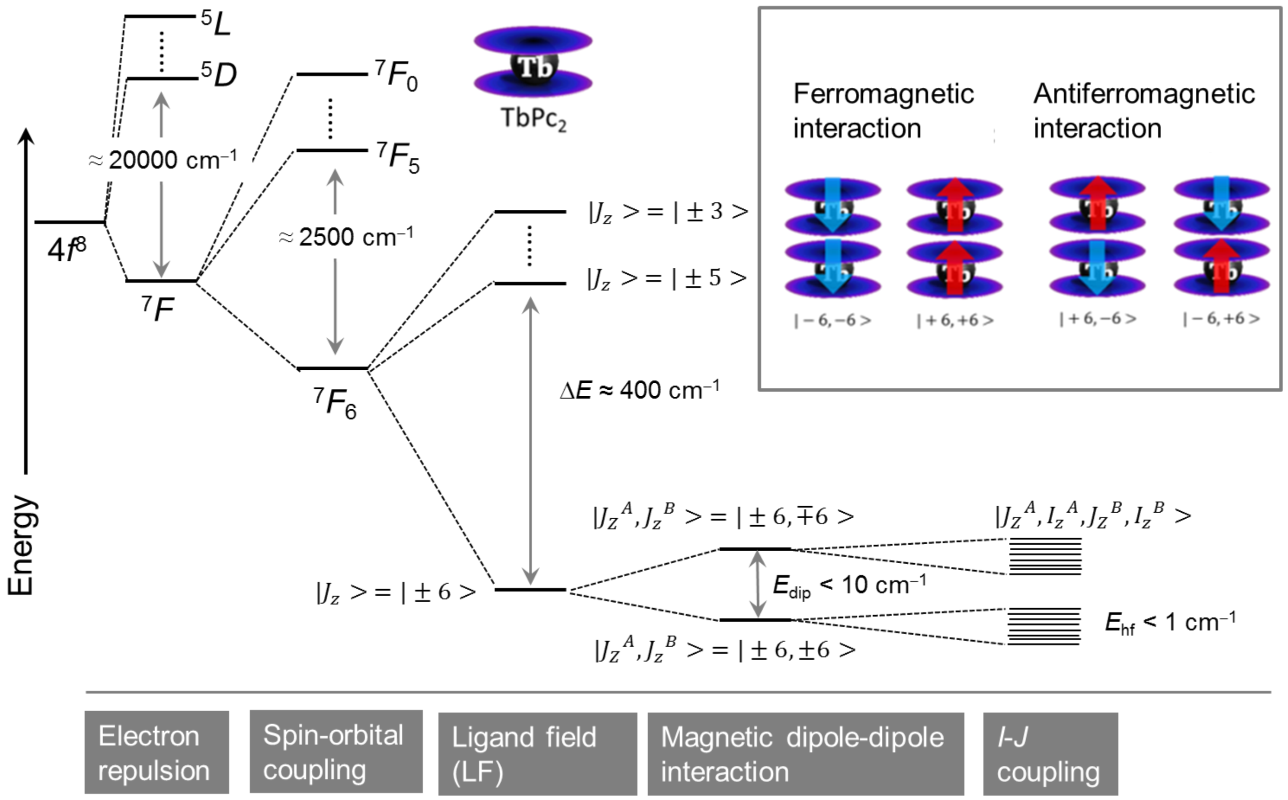

Fig. S29 Schematic representation of electronic structure of Tb^{III} ion ($4f^8$) and TbPc$_2$ complexes. Magnetic dipole-dipole interactions are important for Tb^{III} dinuclear complexes.

The extended Debye model (eq. S8)[7]

$$\chi_{total}(\omega) = \chi_s + (\chi_T - \chi_S)\left[\frac{\beta}{1 + (i\omega\tau_1)^{1-\alpha_1}} + \frac{1-\beta}{1 + (i\omega\tau_2)^{1-\alpha_2}}\right] \qquad \text{(eq. S8)}$$

$$\begin{aligned}\chi' = \chi_S + (\chi_T - \chi_S)&\left\{\frac{\beta\left[1 + (\omega\tau_1)^{1-\alpha_1} sin\, {}^1\!/_2\, \alpha_1\pi\right]}{1 + 2(\omega\tau_1)^{1-\alpha_1} sin\, {}^1\!/_2\, \alpha_1\pi + (\omega\tau_1)^{2(1-\alpha_1)}}\right.\\ &\left. + \frac{(1-\beta)\left[1 + (\omega\tau_2)^{1-\alpha_2} sin\, {}^1\!/_2\, \alpha_2\pi\right]}{1 + 2(\omega\tau_2)^{1-\alpha_2} sin\, {}^1\!/_2\, \alpha_2\pi + (\omega\tau_2)^{2(1-\alpha_2)}}\right\} \qquad \text{(eq. S9)}\end{aligned}$$

$$\begin{aligned}\chi'' = (\chi_T - \chi_S)&\left\{\frac{\beta(\omega\tau_1)^{1-\alpha_1} cos\, {}^1\!/_2\, \alpha_1\pi}{1 + 2(\omega\tau_1)^{1-\alpha_1} sin\, {}^1\!/_2\, \alpha_1\pi + (\omega\tau_1)^{2(1-\alpha_1)}}\right.\\ &\left. + \frac{(1-\beta)(\omega\tau_2)^{1-\alpha_2} cos\, {}^1\!/_2\, \alpha_2\pi}{1 + 2(\omega\tau_2)^{1-\alpha_2} sin\, {}^1\!/_2\, \alpha_2\pi + (\omega\tau_2)^{2(1-\alpha_2)}}\right\} \qquad \text{(eq. S10)}\end{aligned}$$

where χ_S is the adiabatic susceptibility, χ_T is the isothermal susceptibility,[40,50] ω (= $2\pi\nu$) is the angular frequency, τ_1 and τ_2 are the magnetization relaxation times, τ_1 and τ_2 describe the distributions of the relaxation processes, β is the weight of the first relaxation process, and $(1-\beta)$ corresponds to the second one. The real part and the imaginary part are given by equations (eq. S9) and (eq. S10), respectively.

Table S5. Selected geometry and SMM parameters for **1–3** and a related SMM

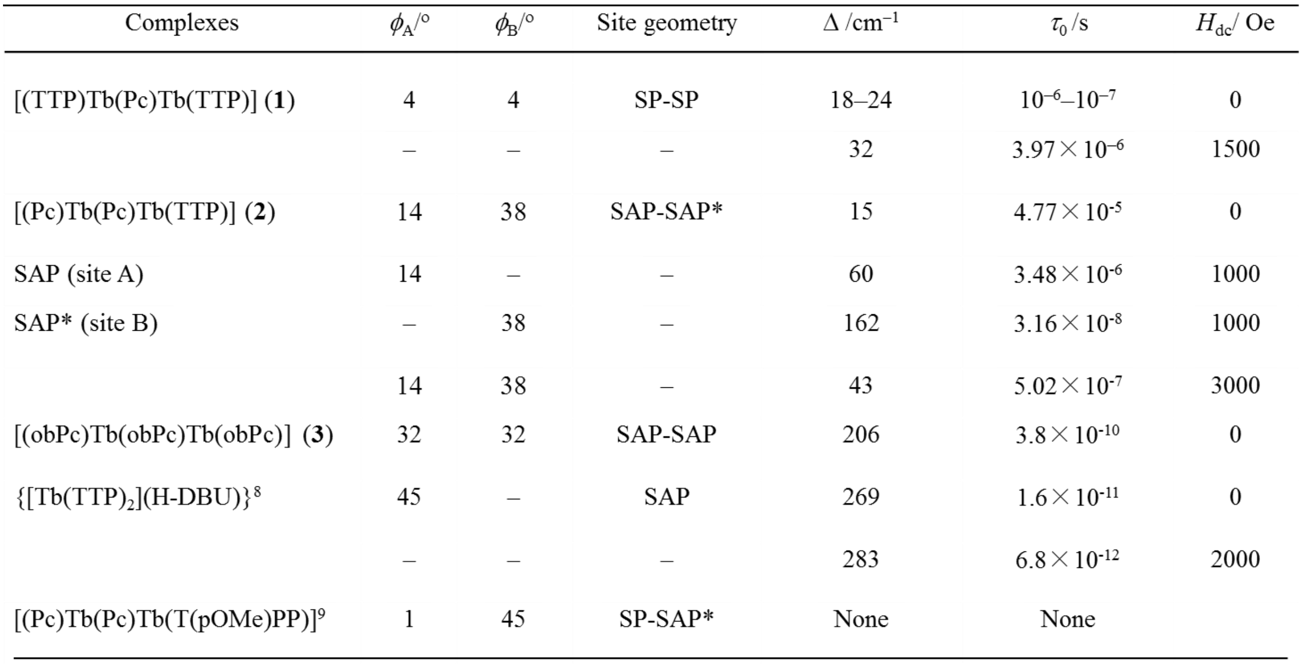

Complexes	ϕ_A/°	ϕ_B/°	Site geometry	Δ /cm^{-1}	τ_0 /s	H_{dc}/ Oe
[(TTP)Tb(Pc)Tb(TTP)] (**1**)	4	4	SP-SP	18–24	10^{-6}–10^{-7}	0
	–	–	–	32	3.97×10^{-6}	1500
[(Pc)Tb(Pc)Tb(TTP)] (**2**)	14	38	SAP-SAP*	15	4.77×10^{-5}	0
SAP (site A)	14	–	–	60	3.48×10^{-6}	1000
SAP* (site B)	–	38	–	162	3.16×10^{-8}	1000
	14	38	–	43	5.02×10^{-7}	3000
[(obPc)Tb(obPc)Tb(obPc)] (**3**)	32	32	SAP-SAP	206	3.8×10^{-10}	0
{[Tb(TTP)$_2$](H-DBU)}[8]	45	–	SAP	269	1.6×10^{-11}	0
	–	–	–	283	6.8×10^{-12}	2000
[(Pc)Tb(Pc)Tb(T(pOMe)PP)][9]	1	45	SP-SAP*	None	None	

The experimental data of **3** from ref. 7e (see main text).

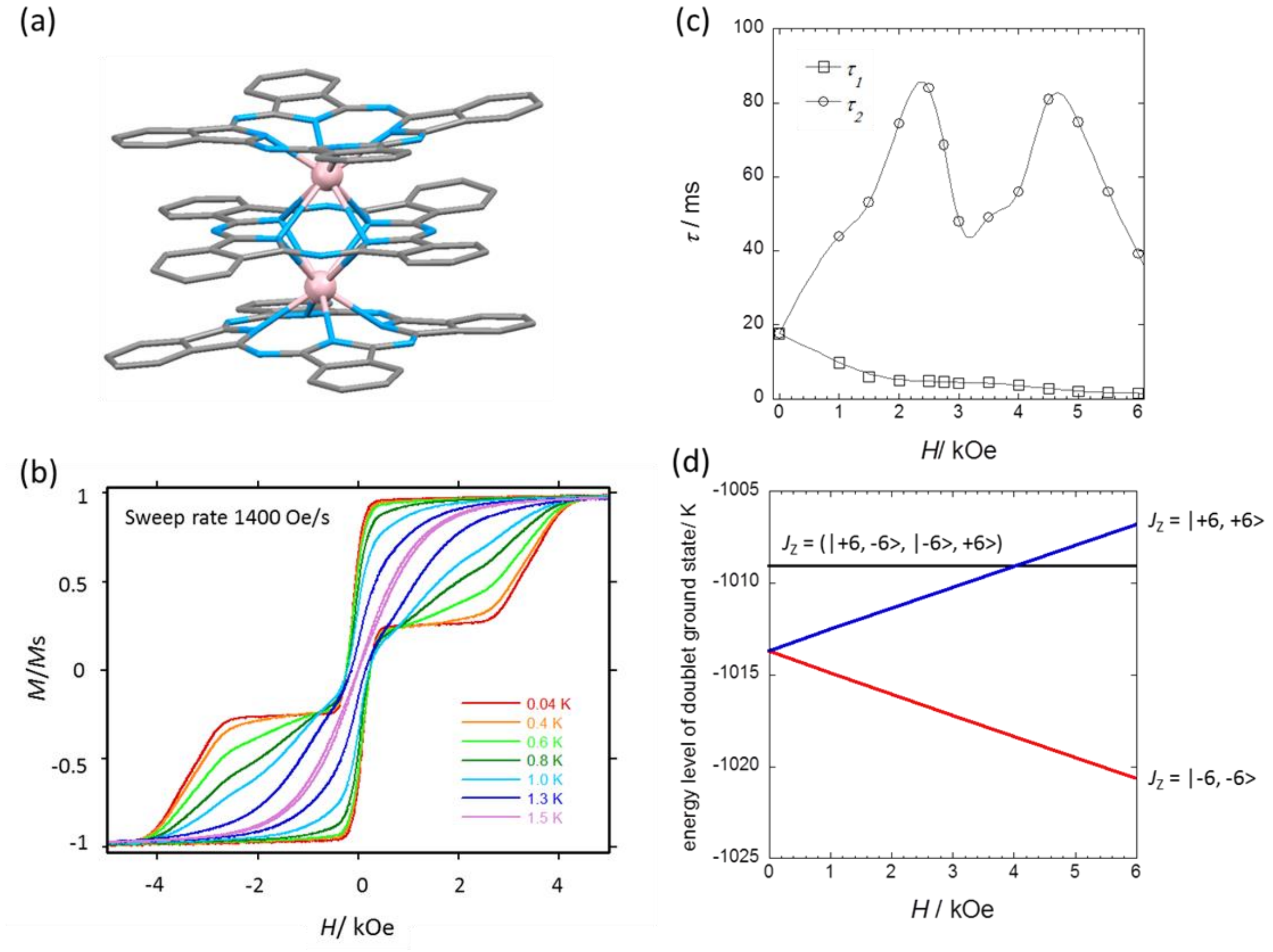

Fig. S30[10] (a) Crystal structure of $Tb_2(obPc)_3$. The *n*-butoxy chains have been omitted for clarity. (b) Hysteresis loops for a single crystal of $Tb_2(obPc)_3$. (c) Relaxation time (τ) versus magnetic field plot for $Tb_2(obPc)_3$ made by using parameters obtained from Argand plots. (d) Zeeman diagram of the doublet ground state for $Tb_2(obPc)_3$ which was obtained from magnetic heat capacity (C_m) in an H_{dc}.

References

1. J. Jiang, D. P. Arnold and H. Yu, *Polyhedron*, 1999, **18**, 2129 and references therein.
2. F. Luis, J. Bartolomé, J. F. Fernández, J. Tejada, J. M. Hernández, X. X. Zhang and R. Ziolo, *Phys. Rev. B*, 1997, **55**, 11448.
3. J. Bartolomé, G. Filoti, V. Kuncser, G. Schinteie, V. Mereacre, C. E. Anson, A. K. Powell, D. Prodius and C. Turta, *Phys. Rev. B*, 2009, **80**, 014430.
4. J. Ferrando-Soria, D. Cangussu, M. Eslava, Y. Journaux, R. Lescouëzec, M. Julve, F. Lloret, J. Pasán, C. Ruiz-Pérez, E. Lhotel, C. Paulsen and E. Pardo, *Chem. Eur. J.*, 2011, **17**, 12482.
5. I. A. Gass, B. Moubaraki, S. K. Langley, S. R. Batten and K. S. Murray, *Chem. Commun.*, 2012, **48**, 2089.
6. K. S. Cole and R. H. Cole, *J. Chem. Phys.*, 1941, **9**, 341.
7. N. Domingo, F. Luis, M. Nakano, M. Muntó, J. Gómez, J. Chaboy and N. Ventosa, Phys. Rev. B, 2009, **79**, 214404-1.
8. D. Tanaka, T. Inose, H. Tanaka, S. Lee, N. Ishikawa and T. Ogawa, *Chem. Commun.*, 2012, **48**, 7796.
9. S. Sakaue, A. Fuyuhiro, T. Fukuda and N. Ishikawa, *Chem. Commun.*, 2012, **48**, 5337.
10. K. Katoh, T. Kajiwara, M. Nakano, Y. Nakazawa, W. Wernsdorfer, N. Ishikawa, B. K. Breedlove and M. Yamashita, *Chem. Eur. J.*, 2011, **17**, 117.